2013-04-05

The Effect of Myostatin on Glucose Metabolism and Insulin Sensitivity

Ghozlan, Mostafa

UNIVERSITY OF CALGARY

The Effect of Myostatin on Glucose Metabolism and Insulin Sensitivity

by

Mostafa Mohamed Mostafa Abdelmageid Ghozlan

A THESIS SUBMITTED TO THE FACULTY OF GRADUATE STUDIES

IN PARTIAL FULFILMENT OF THE REQUIREMENTS FOR

THE DEGREE OF MASTER OF SCIENCE

DEPARTMENT OF BIOCHEMISTRY AND MOLECULAR BIOLOGY

CALGARY, ALBERTA

APRIL, 2013

Abstract

Aim

Myostatin (MSTN) is a negative regulator of skeletal muscle proliferation and differentiation that we previously associated with insulin resistance in humans and mice. We assessed its potential regulatory role in glucose metabolism and insulin sensitivity *in vivo* and *in vitro.*

Methods

Using various approaches we assessed the following parameters: *in vivo* GTT and ITT and *in vitro* insulin-stimulated glucose uptake for insulin sensitivity, qRT-PCR for *Glut1, Glut4, Gyg1, Hk2, IL-6,* Western blotting for protein levels of AMPK and ACC and high-resolution respirometry for glucose-dependent mitochondrial respiration.

Results

MSTN showed significant reduction of hepatic insulin-stimulated glucose uptake *in vitro* and reduced glycogen content *in vivo* without affecting glycolysis, glucose metabolism genes, AMPK signalling or mitochondrial respiration.

Conclusion

This study presents evidence for the potential role of liver in MSTN-induced insulin resistance; especially glucose uptake and glycogen content, which necessitates further investigation of the role of MSTN in this metabolically critical organ.

Acknowledgements

This dissertation would not have been possible without the guidance and the help of many individuals who -by various means- contributed and extended their valuable assistance in the completion of this thesis. It is to them I owe my profound gratitude:

First and foremost, Dr. Dustin Hittel, my supervisor and mentor, for his patience, his unwavering continual guidance and enthusiasm that enabled me to develop an understanding of the subject and for providing me with an excellent environment to conduct my research.

Dr. Jane Shearer and Dr. Raylene Reimer, who accepted to be on my supervisory committee, for their advice and for communicating their valuable knowledge.

Dr. Jill Parnell, for accepting to be on my thesis oral examining committee.

Curtis Hughey, for sharing his expertise in high-resolution respirometry, for offering generous assistance throughout my research and for kindly reviewing this thesis.

Dr. Rani Watts and Virginia Berry, who helped me with various techniques throughout my work and to Elizabeth Gnatiuk for her prompt assistance.

Dr. Julie Deans, the coordinator of the Biochemistry and Molecular Biology Graduate Program, for her great assistance and genuine support.

My friends, my relatives, my professors, my colleagues, my students and all those who supported and encouraged me in any respect during the completion of this research.

My tremendously loving family, for their continual unconditional love and support and for their undivided devotion and commitment.

And above all, God the Almighty, for blessing me with all those inspiring, supportive people and for giving me the privilege to conduct this research and offer this humble contribution.

I heartily would like to dedicate this thesis to:

My utterly loving mom, Dr. Hanaa Eid and my amazingly caring dad, Dr. Mohamed Ghozlan, who kept my spirits up when the muses failed me, for their continual unconditional love and support and for their undivided devotion and commitment.

My beloved brothers: Hassan and Osama Ghozlan.

My best friends and soul mates: Youssef Bacoura, Mai Hamdy, Mostafa Bahbah.

The soul of my late uncle: Awad Ghozlan.

The souls of Dr. Omar Rashwan and Dr. Adel Kheir Eldin.

The souls of all the Egyptians who passed away in the peaceful Revolution of January 25, 2011.

Table of Contents

List of Tables

List of Figures and Illustrations

List of Symbols, Abbreviations and Nomenclature

Symbol	Definition
AAV	Adeno-associated virus
ACC	Acetyl CoA-carboxylase
ActR-IIB	Activin receptor type 2B
AICAR	AICA-riboside; 5-aminoimidazole-4-carboxamide-riboside
AIDS	Acquired immunodeficiency syndrome
ALK4	Activin receptor-like kinase 4; Activin receptor type-1B
ALK5	Activin receptor-like kinase 4; TGF-beta receptor type I
AMP	5’ Adenosine monophosphate
AMPK	AMP-activated protein kinase
ATP	Adenosine 5’-triphosphate
AUC	Area under the curve
BGL	Blood glucose level
BLOTTO	Bovine lacto transfer technique optimizer
BMI	Body mass index
BMP-1	Bone morphogenetic protein
CaMK IV	Calcium/calmodulin-dependent protein kinase type IV
CCR	Coupling control ratio
CD	Chow diet
COX IV	Cytochrome c oxidase; Complex IV.
CTRL	Control
CVD	Cardiovascular diseases

DEPC	Diethylpyrocarbonate
DMEM	Dulbecco's modified Eagle's medium
DPBS	Dulbecco's phosphate-buffered saline
E	Electron transport system respiration
EDTA	Ethylenediaminetetraacetic acid
ETS	Electron transport system
FCCP	Carbonylcyanide-p-trifluoromethoxyphenylhydrazone
FCR	Flux control ratio
FST	Follistatin
FSTL-3	Follistatin-like protein 3
GASP-1	Growth and differentiation factor -associated serum protein 1
GDF 11	Growth differentiation factor
GIR	Glucose infusion rate
GLUT1	Glucose transporter type 1
GLUT4	Glucose transporter type 4
GSK-3	Glycogen synthase kinase 3
GTT	Glucose tolerance test
GYG 1	Glycogenin 1
HEPES	4-(2-hydroxyethyl)-1-piperazineethanesulfonic acid
HFD	High-fat diet
HIV	Human immunodeficiency virus
HK2	Hexokinase 2
HOMA	Homeostatic model assessment

HRR	High-resolution respirometry
IGF-1	Insulin-like growth family 1
IGT	Insulin glucose tolerance
IL-6	Interleukin 6
IP	Intraperitoneal
IR	Insulin resistance
IS	Insulin sensitivity
ITT	Insulin tolerance test
kDa	Kilodalton
L	Leak respiration
Ldlr	Low density lipoprotein receptor
LTBP-3	Latent TGF-beta binding protein-3
MSTN	Myostatin
mTOR	Mammalian target of rapamycin
NMRS	Nuclear magnetic resonance spectrophotometry
NRF-1	Nuclear respiratory factor 1
O2k	OROBOROS Oxygraph 2K
PBS	Phosphate buffered solution
PCP	Phosphorylation control protocol
PEEK	Polyether ether ketone
PGC-1α	Peroxisome proliferator-activated receptor gamma coactivator 1-alpha
PI3K	Phosphatidylinositol 3 kinase

qRT-PCR	Quantitative reverse transcription polymerase chain reaction
R	Routine respiration
RCR	Respiratory control ratio
sActR-IIB	Soluble fraction of activin receptor type 2B
SCL2A1	Solute carrier family 1
SCL2A4	Solute carrier family 4
SDS-PAGE	Sodium dodecyl sulfate polyacrylamide gel electrophoresis
SEM	Standard error of means
T1D	Type 1 Diabetes
T2D	Type 2 Diabetes
TGF-β	Transforming growth factor beta
WHO	World Health Organization
WT	Wild-type

Epigraph

“And of knowledge ye have been vouchsafed but little”

Qur’an; Surat Al-'Isra' [17:85]

Chapter One: **INTRODUCTION**

1.1 Background

1.1.1 Diabetes mellitus

The World Health Organization (WHO) defines "*Diabetes mellitus*" or simply "diabetes" as a chronic disease that occurs either when the pancreas does not produce sufficient insulin (Type 1 diabetes; T1D, insulin-dependent, juvenile or childhood-onset diabetes) or when the body cannot efficiently utilize the insulin it produces (Type 2 diabetes; T2D, non-insulin-dependent or adult-onset diabetes) resulting in an elevated fasting blood glucose level (BGL), leading over time to grave damage to many of the body's systems, particularly the nerves and blood vessels. T2D comprises nearly 90% of people with diabetes worldwide, and is - in part- a result of obesity and physical inactivity. It could be treated with oral medication (WHO September 2012).

1.1.2 Burden and Impact of T2D Worldwide

In 2011, there was an estimate of 366 million persons worldwide afflicted with T2D. It is projected that in 2030, this will have reached 552 million. Moreover, an estimated 280 million people worldwide have an impaired glucose tolerance (IGT); a precursor to diabetes. It is projected that, this will have reached 398 million by 2030; or 7% of the adult population. (IDF 2011). IGT immensely increases the risk of developing T2D (Shaw, Zimmet et al. 1999) and it is linked to the development of cardiovascular disease (CVD) (Perry and Baron 1999, Tominaga, Eguchi et al. 1999).

The greatest number of people with diabetes fell in the age group between 40 to 59 years old. Globally, diabetes caused around 4.6 million deaths in 2011, which exceeded those due to HIV/AIDS, malaria, and tuberculosis combined, thus constituting 8.2% of all-cause mortality. Lower and middle-income countries happened to have the largest share of deaths. At least 458 billion Canadian dollars of the healthcare expenditures worldwide were attributed to diabetes in 2011; i.e. 11% of the entire healthcare expense in adults; ages between 20 and79 (IDF 2011).

1.1.3 Burden and Impact of T2D in Canada

In 2009, the Canadian Diabetes Association commissioned a report to appraise the expense of diabetes to the Canadian healthcare system, and to assess the effect of solutions shown to decrease diabetes incidence and gravity in Canada. The number of diabetic Canadians increased from 1.3 million (4.2% of population) in 2000 to 2.5 million (7.3% of population) by 2010 and will grow to 3.7 million (9.3% of population) by 2020. Consequently, the cost of diabetes in Canada -beyond the great human toll of this disease- will increase from 6.3 billion Canadian dollars/annum in 2000 to 16.9 billion Canadian dollars/annum by 2020 (CDA 2009).

The Public Health Agency of Canada reported that in 2009 more than half of the diabetic Canadians (~1.2 million) were of working age; between 25 and 64 years of age. From 1999 to 2009, the prevalence of diagnosed diabetes amongst Canadians grew by 70%. Slightly less than 50% of the newly diagnosed diabetics were individuals aged 45

to 64 years old, nearly half (47.5%) of these were obese; implying that obesity was a chief contributor to diabetes in this age group (PHAC 2011).

Compared to non-diabetic persons, diabetics are at least 3 times more likely to be hospitalized with CVD, 12 times more likely to be hospitalized with end-stage renal disease, and almost 20 times more likely to be hospitalized with non-traumatic lower limb amputations. T2D was the major reason of 34% of new cases of end-stage renal disease in 2009, causing an increasing need for renal replacement therapy (either transplant or dialysis) in the Canadian health care system. Almost 40% of the diabetic Canadian adults rated their health as "fair" or "poor", versus 10% only of the non-diabetic adult population. Close to 30% of the individuals who died in Canada in 2009 had diabetes, compared to only 3.1% in 2007. Although diabetes itself does not typically lead to death directly, the complications associated with diabetes do. At every age group, the mortality rates showed by individuals with diabetes were at least double those without diabetes, which results in significant decreases in life expectancy as well as health-adjusted life expectancy (PHAC 2011).

Evidently, there is an increased risk of developing T2D as individuals grow in age. Hence a higher incidence of diabetes in Canada is expected as the entire Canadian population ages. In 2006, seniors comprised nearly 14% of the total Canadian population, while in 2031, they will be almost one quarter (24%) of the population. By the year 2056, the median age of citizens in Canada will have grown to 45–50 years and, hence, more than 50% of Canadians will already possess one risk factor at least; i.e. being above 40 years old (StatsCan 2005, CDA 2009).

1.1.4 Insulin Resistance

Insulin resistance (IR), or the reduced response of target tissues - such as skeletal muscle, liver, and adipocytes - to insulin, is attributed to the non-insulin dependent T2D, together with a number of pathological conditions such as CVD and obesity. T2D typically has high insulin levels in order to counterbalance the IR occurring in various target tissues; namely liver, skeletal muscle and adipose tissue. However, the mechanisms linking the progression of IR are not fully characterized yet (Taubes 2009). Interestingly though, studies show that IR in skeletal muscle counts to be the explicit major defect noticed even decades before beta cell dysfunction and obvious hyperglycemia occur (Lillioja, Mott et al. 1988, Warram, Martin et al. 1990). Since skeletal muscle is the predominant tissue where insulin-mediated glucose uptake occurs in the postprandial state, therefore enhancing insulin sensitivity (IS) of skeletal muscle is an essential tool for enhancing IS of the entire body (Savage, Petersen et al. 2007, DeFronzo and Tripathy 2009).

1.1.5 Skeletal Muscle and Myostatin

Skeletal muscle constitutes almost 40% of the lean body weight of adults, thus being the largest organ in non-obese individuals (Pedersen and Febbraio 2012). Mounting evidence shows that skeletal muscle could function as an endocrine organ, thus exhibiting vital metabolic regulatory roles via secreting “myokines”; those are cytokines and other peptides that are synthesized, expressed, and secreted by skeletal muscle where they affect the body in an autocrine, paracrine or endocrine manner (Febbraio and Pedersen

2005, Pedersen and Febbraio 2008, Pedersen 2009). Myokines mediate the metabolic cross-talk between skeletal muscle, liver and adipose tissues in response to exercise and dietary stimuli. Investigating the mechanistic role of myokines will help in elucidating the metabolic regulatory role of skeletal muscle, consequently offering new tools to prevent and/or treat metabolic syndromes due to skeletal muscle dysfunction. Myostatin (MSTN) is a muscle protein that fulfills the criteria of a myokine. MSTN is a secreted protein - belonging to the transforming growth factor β (TGF-β) superfamily - that has been described as a potent negative regulator of skeletal muscles (McPherron, Lawler et al. 1997, Lee 2007). MSTN inhibits myoblast proliferation (Thomas, Langley et al. 2000) and differentiation (Langley, Thomas et al. 2002) as well as inhibiting satellite cell activation and self-renewal (McCroskery, Thomas et al. 2003). MSTN acts on both myoblasts and myotubes, via an anti-differentiation mechanism, which is mediated in part by the perturbation of the IGF-1/Akt/mTOR axis, where IGF-1 was reported to dominantly overcome MSTN inhibition (Trendelenburg, Meyer et al. 2009).

1.1.6 Myostatin and Insulin Resistance

Mstn gene expression was first reported to be increased in skeletal muscle of morbidly obese patients and to subsequently decrease after a loss of fat mass after a procedure of biliopancreatic diversion or gastric bypass surgery (Milan, Dalla Nora et al. 2004, Park, Berggren et al. 2006). Also, *Mstn* mRNA expression increased in the skeletal muscle of first degree relatives of insulin-resistant T2D patients compared to healthy controls (Palsgaard, Brons et al. 2009). Moreover, MSTN protein was secreted at higher

levels in cultured myotubes from extremely obese insulin-resistant female patients compared to those from less obese and normal body weight subjects (Hittel, Berggren et al. 2009). Interestingly, the follow-up work of Hittel *et al.* (2010) showed a strong inverse correlation between plasma MSTN levels and IS suggesting a cause-effect relationship that was further confirmed by inducing IR by injecting mice with recombinant MSTN (Hittel, Axelson et al. 2010). In addition, MSTN-null mice exhibit reduced fat mass and are seemingly resistant to diet-induced IR and hepatosteatosis (fatty liver disease), showing that MSTN inhibition can be favourable to whole body metabolism (Hocquette, Bas et al. 1999, McPherron and Lee 2002, Williams 2004). Finally, a positive correlation between *Mstn* expression and IR in skeletal muscle, regardless of muscle mass, was reported in *ob*/*ob* mice compared to wild-type (WT) mice (Allen, Cleary et al. 2008) suggesting that MSTN signalling has a regulatory role in skeletal muscle metabolism and IR.

1.1.7 AMPK and T2D/IR

Numerous studies aimed at describing the role of AMPK in IS and IR. AMPK or 5' adenosine monophosphate-activated protein kinase is a heterotrimeric serine/threonine kinase, which acts as a metabolic switch, that orchestrates several intracellular systems including the cellular glucose uptake, glucose transporter 4 (GLUT4) biogenesis, β-oxidation of fatty acids and mitochondrial biogenesis (Bergeron, Russell et al. 1999, Winder 2001, Durante, Mustard et al. 2002, Ojuka 2004, Thomson, Porter et al. 2007). The acute (stimulation of glucose uptake into muscle) and chronic (increase in GLUT4)

effects of skeletal muscle contraction were attributed to AMPK activation. (Hayashi, Hirshman et al. 1998, Kurth-Kraczek, Hirshman et al. 1999, Hayashi, Hirshman et al. 2000, Winder 2000, Ojuka, Jones et al. 2002, Ojuka, Jones et al. 2002) AMPK activation was also shown to increase IS, resulting in an improved insulin-stimulated glucose uptake in skeletal muscle (Fisher, Gao et al. 2002, Iglesias, Ye et al. 2002, Jessen, Pold et al. 2003).

Recent conflicting studies reported different results regarding the role of MSTN in AMPK signalling pathway; where one study reported that addition of recombinant MSTN could activate AMPK thus promoting glucose uptake and glycolysis, and improving IS in skeletal muscle cells (Chen, Ye et al. 2010), whereas a more recent one reported that absence of MSTN leads to increased production and activity of AMPK causing enhanced glucose uptake and improved IS of skeletal muscles in high-fat-fed (HFD), MSTN-deficient mice (Zhang, McFarlane et al. 2011).

1.2 Significance

Given the conflicting nature of the evidence, we intended to elucidate whether MSTN plays a mechanistic and/or regulatory role in the glucose metabolism and IS. The results obtained from this study will help in clarifying the role of MSTN in regulating glucose homeostasis in normal, obese and diabetic individuals and will assist in ongoing efforts to utilize MSTN inhibitors as a novel treatment modality for obesity-associated diseases.

1.3 Hypothesis

Based on the mounting evidence from our laboratory and the literature, we propose that MSTN is a novel regulator of carbohydrate metabolism and insulin sensitivity in skeletal muscle and liver.

1.4 Specific Aims

To test this hypothesis and expand upon previous studies, we aim to:

1. Investigate the role of MSTN in glucose metabolism and insulin sensitivity *in vivo* and *in vitro.*
2. Assess the role of AMPK in MSTN-regulated glucose metabolism *in vivo* and *in vitro.*
3. Evaluate the effect of MSTN on glucose-dependent mitochondrial respiration *in vitro.*

1.5 Presentation

This dissertation comprises 5 chapters: *Chapter 1* delineates a brief introduction to the thesis summarizing the significance, aims and hypothesis of the study. *Chapter 2* focuses essentially on the recent and current literature about the effect of MSTN and its involvement in glucose metabolism and IS. *Chapter 3* explains the various methods and techniques used in the study. *Chapter 4* describes the results obtained in the study. *Chapter 5* discusses thoroughly the findings of the study as well as states the strengths

and limitations of the study, summarizes the overall conclusions and presents the potential future directions. References are listed at the end of the thesis.

Chapter Two: **LITERATURE REVIEW**

2.1 Myostatin

2.1.1 Function

Myostatin (MSTN), a member of the transforming growth factor β (TGF-β) superfamily (McPherron, Lawler et al. 1997), is a potent negative regulator of skeletal muscle growth and differentiation (Lee, Dai et al. 2004, Lee 2007).

The inhibition of MSTN function either pharmacologically or through genetic mutations results in a hypermuscular phenotype in mice (McPherron, Lawler et al. 1997), sheep (Clop, Marcq et al. 2006), dogs (Mosher, Quignon et al. 2007), and cows (McPherron, Lawler et al. 1997). Similar mutations in humans produced hypermuscularity without any obvious deleterious effects (Catipovic 2004, Schuelke, Wagner et al. 2004, Williams 2004), which indicates that the role of MSTN in regulating muscle development is highly conserved across various species. This dramatic increase in skeletal muscle mass is primarily due to a combination of both hypertrophy; an increase in the diameter of individual skeletal muscle fibres, and hyperplasia; an increase in the number of skeletal muscle fibres (McPherron, Lawler et al. 1997, Bellinge, Liberles et al. 2005, Girgenrath, Song et al. 2005, Mendias, Marcin et al. 2006, Amthor, Macharia et al. 2007, McPherron, Huynh et al. 2009). Further confirming this role, the inhibition of MSTN in adult mice could increase skeletal muscle mass (Lee 2004, Patel and Amthor 2005).

MSTN is expressed in both developing and adult skeletal muscle. Exogenous systemic administration of MSTN in adult mice caused a drastic muscle loss, showing the postnatal role of MSTN in the maintenance of completely differentiated muscles (Zimmers, Davies et al. 2002). In postnatal skeletal muscle, MSTN inhibited the proliferation and differentiation of myoblasts and the IGF-1/Akt/mTOR pathway regulating protein synthesis (Ji, Zhang et al. 2008, Hittel, Berggren et al. 2009). *In vitro* studies showed that MSTN could block the myoblasts differentiation into myotubes (Langley, Thomas et al. 2004, Rios, Fernandez-Nocelos et al. 2004, McFarlane, Plummer et al. 2006, Yang, Zhang et al. 2007).

It was reported that skeletal muscle mass from *Mstn*$^{-/-}$ mice is almost double the weight of that from *Mstn*$^{+/+}$ mice (McPherron, Lawler et al. 1997) and that the absolute number of fibers in muscle is highest in *Mstn*$^{-/-}$ mice, followed by *Mstn*$^{+/-}$ then by *Mstn*$^{+/+}$ (Mendias, Marcin et al. 2006). Interestingly, the increased skeletal muscle mass from *Mstn*$^{-/-}$ animals appear to be a result of the prenatal and/or perinatal loss of MSTN function rather than a postnatal one. Studies have shown that MSTN loss of function in mice during or after the neonatal period increases the mass of individual skeletal muscle fibres by almost up to 50%, which is less than the increase occurring in *Mstn*$^{-/-}$ mice. This is because the increased skeletal muscle mass is primarily due to hypertrophy not hyperplasia (Zhu, Hadhazy et al. 2000, Grobet, Pirottin et al. 2003, Girgenrath, Song et al. 2005, Tang, Yan et al. 2007, Welle, Bhatt et al. 2007, Haidet, Rizo et al. 2008, Qiao, Li et al. 2008, Matsakas, Foster et al. 2009, Morine, Bish et al. 2010). However, disrupting MSTN function in *mdx* mouse using an adeno-associated virus (AAV) vector expressing an uncleavable mutated MSTN propeptide, but not follistatin (FST), could

increase the percent of type II fibres compared to control *mdx* mice (Haidet, Rizo et al. 2008, Morine, Bish et al. 2010).

Extensive studies have shown MSTN to be a principal negative regulator of myogenesis and postnatal muscle physiology; yet, further investigation to fully elucidate the precise role of MSTN in skeletal muscle mass regulation is necessary.

2.1.2 Molecular Mechanisms

Like other TGF-β family members, MSTN is synthesized as a full-length 37 kDa precursor that dimerizes into a 75 kDa latent complex. Subsequently, it is proteolytically processed at a dibasic site to yield a mature, biologically active, 25 kDa C-terminal dimer and two inactive 25 kDa N-terminal propeptides. This mature MSTN peptide is then secreted from skeletal muscle cells into the circulation, where it could exert a local or a systemic effect. Various proteins were reported to bind to the active mature MSTN dimer or the inactive unprocessed MSTN dimer.(Hill, Davies et al. 2002, Hill, Qiu et al. 2003). In skeletal muscle, latent TGF-β-binding protein-3 (LTBP3) binds to unprocessed MSTN, thus keeping it in an inactive complex in the extracellular matrix (Anderson, Goldberg et al. 2008). The circulating form of MSTN is typically complexed with the N-terminal propeptide which is proteolytically released by extracellular matrix bound BMP-1, allowing interaction with the cell-bound activin type II receptors. (Thomas, Langley et al. 2000, Hill, Davies et al. 2002, Ricaud, Vernus et al. 2003, Lee 2004, Patel and Amthor 2005, Walsh and Celeste 2005, Carnac, Ricaud et al. 2006, Joulia-Ekaza and Cabello 2007, Souza, Chen et al. 2008).

In vitro and *in vivo* experiments demonstrated that MSTN signalling occurs first by binding to the activin type IIB receptor (ActR-IIB), and at least one other unknown receptor, most likely ActR-IIA (Rebbapragada, Benchabane et al. 2003, Lee 2004, Lee, Reed et al. 2005, Patel and Amthor 2005). Upon activation, ActR-IIs interact with type I receptors activin receptor-like kinase ALK4 or ALK5 (Rebbapragada, Benchabane et al. 2003). These interactions trigger a cell signalling cascade, that phosphorylates and activates the canonical transcription factors Smad2 and Smad3, which then translocate inside the nucleus inducing MSTN-specific gene regulation (Thies, Chen et al. 2001, Langley, Thomas et al. 2002, Rebbapragada, Benchabane et al. 2003, LeBrasseur, Schelhorn et al. 2009). Interestingly, the C-terminal mature region of growth differentiation factor 11 (GDF11) shows 90% amino acid sequence homology to MSTN, consequently, GDF11 can signal through ActR-IIB and FST can inhibit receptor binding (Gamer, Wolfman et al. 1999, Lee 2004, Patel and Amthor 2005). Similarly, activins can signal via the ActR-II and ActR-IIB receptors and can be inhibited by FST and follistatin-like protein 3 (FSTL3) (Tsuchida, Nakatani et al. 2004)

Numerous studies investigated the post-developmental role of MSTN in WT adult mice, via intraperitoneal administration of proteins that prevent binding of MSTN to its receptors, namely; a mutated uncleavable propeptide, a soluble ActR-IIB/Fc fusion protein (sActR-IIB) and neutralizing monoclonal antibodies (Whittemore, Song et al. 2003, Wolfman, McPherron et al. 2003, Lee, Reed et al. 2005, LeBrasseur, Schelhorn et al. 2009, Bernardo, Wachtmann et al. 2010). This post-developmental inhibition was also performed via systemic administration of recombinant AVV vector expressing a mutated MSTN propeptide (Bartoli, Poupiot et al. 2007, Foster, Graham et al. 2009, Matsakas,

Foster et al. 2009), or encoding *FST*, *FSTL3*, or *GASP1* genes (Haidet, Rizo et al. 2008), as well as using Cre/LoxP system to knock out *Mstn* gene (Welle, Bhatt et al. 2007).

Noteworthy, the genes for *Mstn*, its receptor *ActR-IIB*, and its inhibitors *FST* and *FSTL3* are expressed in adipose tissue, but considerably less than in skeletal muscle (McPherron, Lawler et al. 1997, Hirai, Matsumoto et al. 2007, Hirai, Matsumoto et al. 2007, Allen, Cleary et al. 2008, Flanagan, Linder et al. 2009). (Figure 2-1)

2.1.3 Regulation and Inhibition

Follistatin (FST) is a secreted autocrine glycoprotein, whose primary function has been determined to be the binding and bioneutralization of the TGF-β superfamily members including MSTN, thus inhibiting the interaction of the latter with ActR-IIB (Lee 2004, Patel and Amthor 2005). Among other regulators of MSTN are the secreted follistatin-like protein 3 (FSTL3) (Hill, Davies et al. 2002), and the growth and differentiation factor-associated serum protein 1 (GASP1), which bind to MSTN in serum thus inhibiting its receptor binding. (Hill, Davies et al. 2002, Hill, Qiu et al. 2003). In skeletal muscle, latent TGF-β-binding protein-3 (LTBP3) maintains full-length MSTN in its inactive latent complex in the extracellular matrix (Anderson, Goldberg et al. 2008).

Numerous studies investigated the post-developmental role of MSTN in WT adult mice, via intraperitoneal administration of proteins that prevent binding of MSTN to its receptors, namely; a mutated uncleavable propeptide, a soluble ActR-IIB/Fc fusion protein (sActR-IIB) and neutralizing monoclonal antibodies (Whittemore, Song et al. 2003, Wolfman, McPherron et al. 2003, Lee, Reed et al. 2005, LeBrasseur, Schelhorn et al. 2009, Bernardo, Wachtmann et al. 2010). This post-developmental inhibition was also performed via systemic administration of recombinant AVV vector expressing a mutated MSTN propeptide (Bartoli, Poupiot et al. 2007, Foster, Graham et al. 2009, Matsakas, Foster et al. 2009), or encoding *FST, FSTL3,* or *GASP1* genes (Haidet, Rizo et al. 2008), as well as using Cre/LoxP system to knock out *Mstn* gene (Welle, Bhatt et al. 2007).

Noteworthy, the genes for *Mstn,* its receptor *ActR-IIB,* and its inhibitors *FST* and *FSTL3* are expressed in adipose tissue, but considerably less than in skeletal muscle

(McPherron, Lawler et al. 1997, Hirai, Matsumoto et al. 2007, Hirai, Matsumoto et al. 2007, Allen, Cleary et al. 2008, Flanagan, Linder et al. 2009). (Figure 2-1)

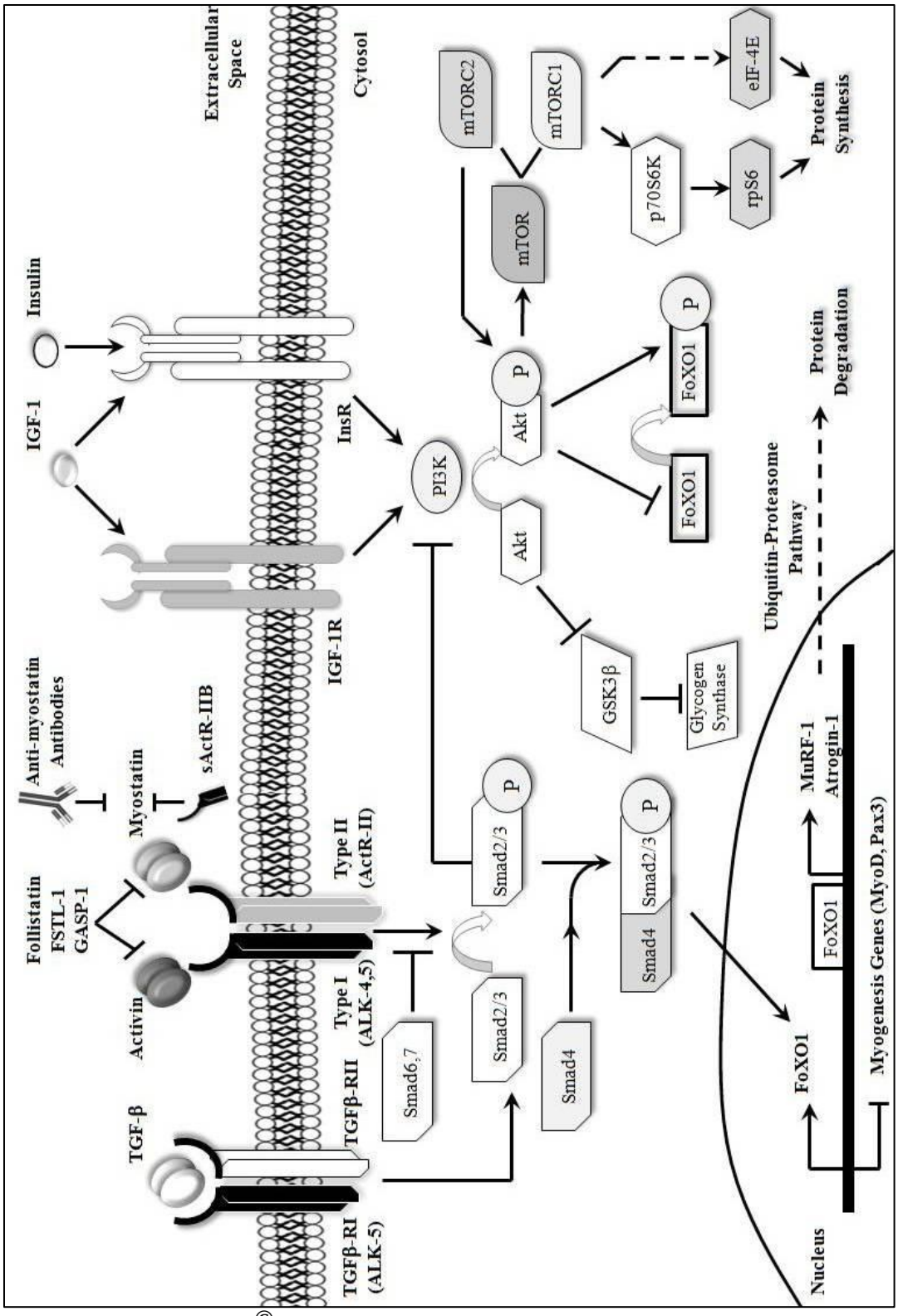

Figure 2-1: Schematic © for myostatin signalling pathway, targets, effectors and inhibitors.

2.2 Effects on Metabolism

2.2.1 Lipid Metabolism

There are conflicting reports about the effect of MSTN inhibition on lipid metabolism. MSTN-null mice showed significantly lower serum cholesterol, as well as reduced serum and hepatic triglyceride levels compared to WT mice (McPherron and Lee 2002, Guo, Jou et al. 2009). MSTN-null cattle showed similar results, however it was not known whether this is caused due to a reduction in intermuscular adipocyte or in intramyocellular lipid (Menissier 1982), where increase of the latter was shown to be a risk factor in the development of IR (Savage, Petersen et al. 2007).

Similarly, treatment of WT adult mice with the sActR-IIB for 10 weeks, drastically lowered fat mass, improved IS and increased muscle glucose uptake but not after 4 weeks (Akpan, Goncalves et al. 2009). Conversely, Benny Klimek *et al*. reported high abdominal fat pad mass in response to MSTN inhibition via injecting a CHO cell line secreting sActR-IIB in athymic nude mice (Benny Klimek, Aydogdu et al. 2010), whereas MSTN inhibition via injecting a DNA vaccine against MSTN showed an increase in skeletal muscle mass without any reduction in abdominal fat pad mass (Tang, Yan et al. 2007).

On the other hand, Zimmers *et al.* showed that the systemic overexpression of MSTN in adult mice induces significant fat loss (Zimmers, Davies et al. 2002), whereas Stolz *et al*. reported that the administration of exogenous MSTN over a range of doses (2-120 ug/day) could not reduce the fat mass in WT or genetically obese (ob/ob, db/db) mice (Stolz, Li et al. 2008). Taken together, these reports suggest contradictory effects of

MSTN inhibition on lipid metabolism. However, the experiments conducted by the systemic administration of MSTN inhibitors into mouse models of obesity suggest that anti-MSTN therapy might be effective in the improvement of glucose metabolism rather than the treatment of frank obesity.

Studies on *Mstn* transgenic mice showed that the extent to which adiposity is affected appears to be inversely proportional to the extent of muscle hypertrophy or atrophy (Sutrave, Kelly et al. 1990, Musaro, McCullagh et al. 2001, Reisz-Porszasz, Bhasin et al. 2003, Pursel, Mitchell et al. 2004, Izumiya, Hopkins et al. 2008, Leong, Kee et al. 2010). Guo *et al* (2009) reported that the enhanced glucose uptake and improved IS, and the concomitant decrease in adipose tissue mass in MSTN-null mice are indirect consequences of the metabolic alterations in skeletal muscle (Guo, Jou et al. 2009). These reports suggest that MSTN does not affect adipose mass directly, and that the effects of MSTN inhibition in reducing adipose mass in the null mice are an indirect result of the increased skeletal muscle mass.

It was reported that MSTN promoted resistance to HFD-induced obesity in transgenic mice, where it improved glucose tolerance and reduced fasting glucose, insulin, and triglycerides levels. MSTN could directly inhibit lipid accumulation, affecting adipose mass, via adipose-specific MSTN overexpression (Feldman, Streeper et al. 2006) rather than muscle-specific MSTN suppression (Guo, Jou et al. 2009). This resistance was attributed to an increased metabolic rate caused by the smaller and apparently immature adipocytes (Feldman, Streeper et al. 2006). Taken together, these results indicate that MSTN signaling in adipocytes does not necessarily have a direct regulatory effect on the

adipose mass in mice fed with CD or HFD; nonetheless they propose a potential role for MSTN in the regulation of adipocyte metabolism.

Increased skeletal muscle mass was reported to indirectly change metabolism of liver as well as adipose tissue. The induction of *Akt* transgene in diet-induced obese mice resulted in decreased body weight and fat mass as well as reduced hepatic steatosis. Akt-mediated skeletal muscle growth protected the liver from the effects of HFD and increased hepatic fatty acid oxidation (Izumiya, Hopkins et al. 2008). These mice likely had increased hepatic fatty acid beta-oxidation due to a higher glucose-dependent energy demand by the hypertrophied skeletal muscle. Likewise, an *in vitro* study showed increased fatty acid oxidation in the mitochondria isolated from livers of $Mstn^{-/-}$, $Ldlr^{-/-}$ double mutant mice fed HFD compared to $Mstn^{+/+}$, $Ldlr^{-/-}$ mice (Tu, Bhasin et al. 2009). On the other hand, there was no increase in hepatic fatty acid oxidation in MSTN-null mice fed HFD (Guo, Jou et al. 2009), neither in MSTN-null mice fed chow diet (CD) (Stolz, Li et al. 2008) nor adult obese (*db/db*) mice receiving anti-MSTN antibody (Stolz, Li et al. 2008). Therefore, hepatic fatty acid oxidation does not seem to be a consistent hallmark of the MSTN-mediated resistance to HFD-induced obesity, where other factors might be contributive e.g. diet composition and length of time on HFD. Nonetheless, it is evident that MSTN plays a role in regulating lipid metabolism in liver.

2.2.2 Glucose Metabolism

Since skeletal muscle is the predominant tissue where insulin-stimulated glucose uptake takes place in the postprandial state, enhancing IS of skeletal muscle is essential

for improving the IS of the entire body (Savage, Petersen et al. 2007, DeFronzo and Tripathy 2009).

MSTN-null mice showed higher glucose utilization and improved IS when measured by indirect calorimetry, glucose and insulin tolerance tests, as well as hyperinsulinemic-euglycemic clamps compared to WT mice (McPherron and Lee 2002, Guo, Jou et al. 2009). Since, the glucose infusion rate (GIR) measured by these clamp studies determines the IS (DeFronzo, Tobin et al. 1979), a high GIR in MSTN-null mice indicates higher glucose uptake by peripheral tissues in response to insulin compared to WT mice (Guo, Jou et al. 2009). Furthermore, *in vivo* administration of insulin in MSTN-null mice resulted in greater activation of Akt, a serine-threonine kinase mediating the signalling of insulin, and insulin-like growth factor 1 (IGF-1), in skeletal muscles, as well as white and brown adipose tissue. This observation (Guo, Jou et al. 2009) suggests that the improvement in whole body IS in MSTN-null mice is not exclusively a result of the increase in skeletal muscle mass (Savage, Petersen et al. 2007, DeFronzo and Tripathy 2009). Interestingly, MSTN was reported to reduce IGF1-induced Akt signalling where it inhibits myoblast differentiation and myotube hypertrophy (Morissette, Cook et al. 2009, Trendelenburg, Meyer et al. 2009). Furthermore, the insulin-stimulated Akt phosphorylation was significantly decreased in both skeletal muscle and liver of MSTN-treated mice together with a profound reduction in IS. (Hittel, Axelson et al. 2010). These results were confirmed by the findings showing increased p-Akt levels in MSTN-null muscles, and even greater levels of insulin-stimulated p-Akt when compared with WT muscles (Zhang, McFarlane et al. 2011).

In summary, despite the growing body of evidence showing that MSTN regulates glucose homeostasis i.e. uptake, utilization and metabolism, the molecular mechanisms need further investigation.

2.2.2.1 AMPK

2.2.2.1.1 Function

AMPK or 5' adenosine monophosphate-activated protein kinase (a.k.a protein kinase, AMP-activated, beta 1 non-catalytic subunit; PRKAB1); is a heterotrimeric serine/threonine kinase, that comprises a catalytic α-subunit and regulatory β- and γ-subunits (Ruderman, Saha et al. 1999, Hawley, Boudeau et al. 2003, Steinberg, Macaulay et al. 2006). In skeletal muscle, α2 is the predominant catalytic isoform, which together with β2 and γ3 subunits constitute a heterotrimeric complex (Davies, Helps et al. 1995, Martin, Alquier et al. 2006). AMPK acts as a metabolic switch, that regulates numerous metabolic processes including; cellular glucose uptake, glucose transporter 4 (GLUT4) biogenesis, β-oxidation of fatty acids, and mitochondrial biogenesis (Bergeron, Russell et al. 1999, Winder 2001, Durante, Mustard et al. 2002, Ojuka 2004, Thomson, Porter et al. 2007).

2.2.2.1.2 Signalling

AMPK activation is triggered by acute increases in the cellular AMP/ATP ratio, such as the increase that happens due to the energy depletion or metabolic stress following exercise (Carling and Hardie 1989, Corton, Gillespie et al. 1994, Yamauchi, Kamon et al.

2002) or during conditions such as hypoxia, ischaemia or osmotic stress (Fujii, Jessen et al. 2006). Upon low intracellular ATP levels, AMPK inactivates anabolic ATP-consuming pathways, including glycogen, fatty acid, and protein synthesis. On the other hand, AMPK activates catabolic ATP-regenerating pathways, including glucose transport, glycolysis and fatty acid oxidation.

Recent studies demonstrated that the acute and chronic effects of skeletal muscle contraction; i.e. the stimulation of glucose uptake into muscle and increase in GLUT4 respectively, could be attributed to AMPK activation. Ojuka *et al.* provided an evidence that elevated cytosolic $Ca^{(2+)}$ and AMPK activation - both of which occurring in exercising muscle - could increase GLUT4 protein in myocytes and skeletal muscles (Ojuka, Jones et al. 2002, Ojuka, Jones et al. 2002). Both contracting and AICAR-perfused muscles were shown to have a significant increase in AMPK activity, glucose uptake, and GLUT4 translocation in skeletal muscles. Insulin-perfused muscles were reported to have significantly enhanced glucose uptake and increased GLUT4 translocation, however there was no significant change in the activation of AMPK compared to the basal levels. It was hypothesized that AMPK could be a key mediator of the insulin-independent glucose transport, thus facilitating glucose uptake in metabolically-stressed, energy-depleted muscle cells in order to regenerate its ATP stores (Hayashi, Hirshman et al. 1998, Kurth-Kraczek, Hirshman et al. 1999, Hayashi, Hirshman et al. 2000, Winder 2000). Activation of AMPK was also shown to increase IS resulting in an improved insulin-mediated glucose uptake in skeletal muscle (Fisher, Gao et al. 2002, Iglesias, Ye et al. 2002, Jessen, Pold et al. 2003).

AICAR or AICA-riboside, is 5-aminoimidazole-4-carboxamide-riboside; an adenosine analog whose injection can artificially activate non-exercising muscles by being taken up into muscles and phosphorylated to form AICA-ribotide (ZMP; an analog of 5'-AMP) that activates AMPK without altering the levels of the nucleotides (Zhang, Frederich et al. 2006, Kristiansen, Solskov et al. 2009).

2.2.2.1.3 Myostatin and AMPK

The recent work of Chen *et al.* reported the first experimental evidence that recombinant MSTN could activate the AMPK signal pathway thus promoting glucose uptake and glycolysis, in C2C12 skeletal muscle cells (Chen, Ye et al. 2010). On the contrary, Zhang *et al.* showed for the first time that MSTN inactivation results in increased AMPK levels and activity causing increased glucose uptake and improved IS of skeletal muscles in HFD, MSTN-deficient mice. They further showed that treatment with sActR-IIB, antagonizing MSTN, could reduce IR in HFD mice (Zhang, McFarlane et al. 2011). These results, although contradictory, suggest that the metabolic switch AMPK has a role the in MSTN-mediated effects on glucose metabolism in skeletal muscle and liver.

2.2.3 Insulin Resistance

There were conflicting studies about the direct effect of MSTN treatment, in the absence of insulin, on glucose uptake in the placenta, where MSTN treatment was reported to increase glucose uptake in human placental extracts (Mitchell, Osepchook et al. 2006), while it inhibited glucose uptake in the choriocarcinoma placental cell line; BeWo cells (Antony, Bass et al. 2007).

In addition, there were contradictory results regarding the effect of MSTN on insulin-dependent glucose uptake in skeletal muscle. Chen *et al.* reported that the direct treatment with recombinant MSTN could promote AMPK-dependent glucose uptake and increase glycolysis in C2C12 skeletal muscle cells (Chen, Ye et al. 2010). In contrast, Zhang *et al* reported that MSTN depletion leads to increased AMPK levels and activity resulting in increased glucose uptake and improved IS in skeletal muscles of MSTN-deficient mice on HFD (Zhang, McFarlane et al. 2011). Furthermore, they showed that MSTN inhibition, using sActR-IIB, could reduce IR in mice on HFD (Zhang, McFarlane et al. 2011).

Several reports showed a positive correlation between *Mstn* expression and IR in skeletal muscles, regardless of muscle mass. *Mstn* mRNA expression increased in first degree relatives of T2D patients, having obvious IR measured by a hyperinsulinemic-euglycemic clamp, compared to healthy controls matched for fat free mass and BMI (Palsgaard, Brons et al. 2009). In addition, *Mstn* protein was secreted at higher levels in cultured myotubes from extremely obese female patients (BMI ~ 49 kg/m^2) compared to those from less obese (BMI = 25 - 40 kg/m^2) and to normal body weight subjects. The

extremely obese females showed higher Homeostasis Model Assessment levels (HOMA) indicating higher insulin resistance (Hittel, Berggren et al. 2009). Results from these studies confirm previous observations of decreased *Mstn* gene expression in skeletal muscle from morbidly obese patients after the decrease of fat mass achieved by biliopancreatic diversion or gastric bypass surgery (Milan, Dalla Nora et al. 2004, Park, Berggren et al. 2006).

Interestingly, the follow-up work of Hittel *et al.* (2010) showed a strong inverse correlation between plasma MSTN levels and IS suggesting a cause-effect relationship that was further confirmed by inducing IR by injecting mice with recombinant MSTN (Hittel, Axelson et al. 2010).

In accordance, *Mstn* gene expression increased in *ob*/*ob* mice compared to WT mice, (Allen, Cleary et al. 2008) in non-mutant mice on HFD versus CD (Allen, Cleary et al. 2008). Taken together, these results imply that MSTN signalling could play a direct regulatory role in skeletal muscle metabolism in addition to an indirect regulatory role on muscle mass.

Data from gene expression studies show a possible role for MSTN signalling in adipose tissue in response to obesity. A study showed that *Mstn* expression increased in subcutaneous adipose tissue from mice on HFD compared to CD (Allen, Cleary et al. 2008). In addition, *Mstn* and *ActR-IIB* expression levels were higher in adipose tissue (Allen, Cleary et al. 2008), whereas *FSTL3* expression was lower in the visceral adipose tissue from *ob*/*ob* mice compared to WT mice (Allen, Cleary et al. 2008). Confirming the latter observation, *FSTL3* knockout mice showed decreased visceral fat pad mass, even though their body composition was comparable to WT mice (Mukherjee, Sidis et al.

2007). In accordance with these results, adipose-specific *Mstn* overexpression in transgenic mice resulted in reduced adipocytes size and increased IS (Feldman, Streeper et al. 2006). Further investigation showed that severe MSTN deficiency in *Mstn* $^{Ln/Ln}$ mice on HFD protects muscle and liver against obesity-induced IR. Moreover, short-term administration of recombinant MSTN in *Mstn* $^{Ln/Ln}$ mice led to increased plasma TNF-alpha and IR (Wilkes, Lloyd et al. 2009).

2.3 Mitochondria

2.3.1 AMPK and Mitochondria

Studies showed that AMPK activation using AICAR could significantly increase the mitochondrial enzymes; cytochrome c, citrate synthase, and malate dehydrogenase in rat quadriceps muscles, as well as increasing GLUT4 and hexokinase activity (Winder, Holmes et al. 2000). These results suggest that the increased AMPK activity associated with exercise-induced muscle contraction might have a role in some of the biochemical adaptations in response to chronic metabolic stress. AMPK was further shown to promote mitochondrial biogenesis and expression of respiratory proteins, by increasing cytochrome c content and muscle mitochondrial density, through the activation of Nuclear respiratory factor 1 (NRF-1) (Bergeron, Ren et al. 2001). NRF-1 is a transcription factor responsible for the expression of key regulatory genes necessary for mitochondrial respiration, and mitochondrial DNA transcription and replication.

Zong *et al.* showed that AMPK activation in skeletal muscle is essential for mitochondrial biogenesis in response to metabolic stress involving chronic energy

depletion as well as the role that AMPK plays in increasing the expression of calcium/calmodulin-dependent protein kinase type IV; CaMK IV and peroxisome proliferator-activated receptor gamma coactivator 1-alpha; PGC-1α which regulates genes responsible for energy metabolism. These findings suggest that, being an energy-sensor, AMPK could be the first signalling step that ties in the acute and the chronic metabolic adaptations in response to cellular energy deficiency; i.e. respectively increased glucose transport, beta-oxidation of fatty acids and increased mitochondrial biogenesis (Zong, Ren et al. 2002).

2.3.2 Myostatin and Mitochondria

Several studies revealed that MSTN deficiency is associated with a reduction in mitochondrial content in skeletal muscle fibres thus impairing the mitochondrial oxidative capacity (Amthor, Macharia et al. 2007, Lipina, Kendall et al. 2010, Savage and McPherron 2010). However, this reduction was explained to be partially due to the decreased ratio of oxidative fibers in MSTN-deficient muscles (Girgenrath, Song et al. 2005, Steelman, Recknor et al. 2006). Furthermore, Baligand *et al.* reported that after electro-stimulated exercise in MSTN-deficient mice, phosphorus nuclear magnetic resonance spectroscopy (^{31}P-NMRS) revealed a reduced oxidative mitochondrial capacity (Baligand, Gilson et al. 2010). A recent study using high-resolution respirometry has shown that lack of MSTN, in MSTN knockout mice, induced a reduction in the coupling of intermyofibrillar mitochondrial respiration which indicates a reduced mitochondrial oxidative capacity, as well as inducing a remarkably higher basal oxygen consumption

compared to WT mice, given that neither lysis of mitochondrial cristae nor excessive swelling were noticed (Ploquin, Chabi et al. 2012). Taken together, we expected that the aforementioned MSTN-associated increase in AMPK-mediated glycolysis (Chen, Ye et al. 2010) would likely result in a shift in mitochondrial respiration which –in turn- would be reflected in a reduction in glucose-dependent oxidative metabolism.

2.4 Objectives

In addition to the indirect effect of MSTN on metabolism by regulating muscle mass, there is mounting evidence that MSTN plays a direct role in the metabolism of skeletal muscle and liver. In this study, we will explore the link between MSTN and carbohydrate metabolism *in vivo* and *in vitro* using a variety of investigative techniques. Specifically, we intend to investigate the role of MSTN and AMPK in glucose metabolism *in vivo* and *in vitro,* and determine the effect of MSTN on IS. In addition, we will evaluate the effect of MSTN on glucose-dependent mitochondrial respiration *in vitro* to have a better understanding of the oxidative capacity upon treatment with MSTN.

Chapter Three: **METHODOLOGY**

3.1 Chemicals

3.1.1 Antibodies

The primary antibodies for Acetyl-CoA Carboxylase, phospho-Acetyl-CoA Carboxylase (Ser79), Akt (pan)(C67E7), phospho-Akt(Ser473)(D9E), AMPK-alpha, phospho-AMPK-alpha (Thr172), Cytochrome oxidase; COX IV (3E11) Rabbit mAb, Smad2/3 and phopho-Smad2 (Ser465/467) were purchased from Cell Signaling Technology (Beverly, USA). Alpha-smooth muscle Actin was purchased from Sigma-Aldrich Co. (Saint-Louis, USA). The secondary antibody for all primary antibodies was a horseradish peroxidase-linked, purified goat anti-rabbit IgG purchased from Cell Signaling Technology.

3.1.2 Myostatin

Recombinant myostatin (MSTN) was purchased from R&D Systems (Minneapolis, USA) for *in vivo* experiments and from PeproTech (Rocky Hill, USA) for *in vitro* experiments.

3.2 Animal Model

3.2.1 Ethics

All experiments were conducted following the approval (# BI09R-45) of the protocol by the University of Calgary Animal Care and Use Committee and abide by the Canadian Association for Laboratory Animal Science guidelines for animal experimentation.

3.2.2 Animals

Twelve four-week old male C57/Bl6 littermate mice were obtained from the Health Sciences/Life and Environmental Sciences Animal Resource Centre in the University of Calgary.

Mice were segregated randomly in regular cages supplied with Aspen Chip bedding; heat-treated, aspirated aspen hardwood laboratory bedding (NEPCO, Warrensburg, USA). Mice were kept in controlled rooms with a 12:12 hours light-dark cycle, at 23-24°C with access to chow and water *ad libitum* for 24 hours prior to any experiment.

3.2.3 Glucose Tolerance Test and Insulin Tolerance Test

On the morning of every experiment day, all beddings, chow and water in all cages were discarded and replaced with new clean ones. Mice in the cages were introduced to the lab and were allowed to acclimatize for an hour prior to the beginning of any experiment. Mice were fasted at 9 am for four hours before performing any Glucose Tolerance Test (GTT) or Insulin Tolerance Test (ITT). Using a Mettler Toledo Precision Balance (Thermo Fisher Scientific Inc., Rockford, USA) mice were weighed twice; once

upon introducing cages to the lab and once directly before starting experiments. Both weights were recorded, where the latter was used to calculate doses.

Mice were divided into two groups; a control group and a test group, each comprising six mice. In the control group, mice received an intraperitoneal (IP) injection (100ul/mouse) of isotonic phosphate-buffered saline (PBS) of pH 7.4 (Life Technologies Inc., Burlington, Canada), whereas in the test group, mice received an IP injection of a supra-physiological dose (2ug/mouse/day) (Stolz, Li et al. 2008) of recombinant MSTN (R&D Systems) that was diluted in 100ul of PBS used as a vehicle as in the control group.

Mice in control and test groups were, respectively, injected with PBS and recombinant MSTN two hours prior to GTTs or ITTs. All IP injections were done using sterile 1 ml insulin syringe with an Ultra-Fine™ needle (BD-Canada, Mississauga, Canada) in order to minimize the potential discomfort at the site of injection. Mice were injected with PBS or recombinant MSTN for five consecutive days, where GTT was performed on day "5" of the IP injections and ITT on day "6".

3.2.4 Blood Collection

Blood for GTT and ITT was collected by obtaining a blood drop from the tail vein by inducing a minimal cut at the tail tip using a surgical blade. The blood drop was used immediately on OneTouch ®Ultra® Test Strips (LifeScan Europe, Zug Switzerland), where blood glucose level (BGL) was determined using the blood glucose meter OneTouch®UltraSmart® (LifeScan). BGL was determined at five time-points, namely:

0, 15, 30, 60 and 120 minutes after the IP administration of glucose in GTTs or insulin in ITTs.

3.2.5 Tissue Collection

On the sixth day, mice were euthanized using an IP injection (200 mg/kg body weight) of sodium pentobarbital solution (Ceva Santé Animale, Libourne, France), followed by prompt cervical dislocation. The livers and gastrocnemius muscles were isolated, dried on Kimwipes® (VWR*)*, and the wet weight was determined using Mettler HK160 Analytical Balance (Thermo Fisher Scientific). Organs were collected in microtubes, immediately frozen in liquid nitrogen (Praxair Distribution Inc., Calgary, Canada), and stored at -80°C for later analysis.

3.2.6 Tissue Homogenates

A piece of the liquid-frozen tissues was brought to a porcelain mortar, where it was pulverized in the presence of liquid nitrogen with a porcelain pestle. The pulverized tissue was swiftly transferred to previously weighed microtubes. The microtubes were weighed using Mettler HK160 Analytical Balance (Thermo Fisher Scientific) and the tissue weight was determined. Ice-cold fresh modified PI3K/GSK-3 Buffer (Recipe: 10% glycerol, 150 mM NaCl, 50 mM HEPES (pH 7.5), 1% NP-40, 2 mM EDTA (pH 8.0), 1 mM $CaCl_2$, 1 mM $MgCl_2$, 3 mM benzamide, 1X SIGMAFAST™ Protease Inhibitor (Sigma-Aldrich), 1X ProteaseArrest™ (G-Biosciences, Saint-Louis, USA)) was added to the pulverized tissue in the ratio of 20:1 (20ul buffer to 1 mg tissue). The microtubes

were rotated end-over-end for 24 hours at 4°C. Microtubes were subsequently centrifuged for 20 minutes at 4°C and a speed of 14000 rpm using Microfuge® 22R Refrigerated Microcentrifuge, (Beckman Coulter Canada Inc., Mississauga, Canada). The supernatants were collected into new microtubes, whereas the residual pellets were discarded. Total protein concentrations were determined colourimetrically in a 96-well plate using Pierce BCA ™ Protein Assay Kit (Thermo Fisher Scientific). Optical densities were measured using SpectraMax® 190 Absorbance Microplate Reader and SoftMax Pro Microplate Data Acquisition & Analysis Software (Molecular Devices, Sunnyvale, USA).

3.3 Cell Culture

C2C12 murine myoblasts and Hepa-1C1C7 murine hepatoma cells were purchased from American Type Culture Collection (Manassas, USA). For proliferation, cells were plated in Greiner CELLSTAR® 75cm² Cell Culture Flasks (Greiner Bio-One, Frickenhausen, Germany) using "Proliferating Medium" composed of; Dulbecco's Modified Eagle's Medium (DMEM) [high glucose (25 mM), with L-glutamine (4mM)] (Life Technologies), supplemented with 10% (v/v) One Shot ™ Fetal Bovine Serum (Life Technologies), and 1% (v/v) antibiotic antimycotic solution [10000 Unit Penicillin, 10 mg Streptomycin, 25 ug Amphotericin B per ml] (Sigma-Aldrich) and incubated in Forma Series II 3110 Water-Jacketed CO_2 Incubator (Thermo Fischer Scientific) providing a humidified atmosphere of 95% air and 5% CO2 at 37 °C.

For differentiation of myoblasts into myotubes, confluent myoblasts were grown for 3 days (72 hours) in "Differentiating Medium" composed of; DMEM [high glucose (25

mM), with L-glutamine (4mM)] (Life Technologies), supplemented with 5% (v/v) heat-inactivated Horse Serum (Life Technologies), and 1% (v/v) antibiotic antimycotic solution [10000 Unit Penicillin, 10 mg Streptomycin, 25 ug Amphotericin B per ml] (Sigma-Aldrich) and incubated in the CO_2 incubator.

For sub-culturing myoblasts, myoblasts in the cell culture flasks were trypsinized using TrypLE™ Express as follows: cells were gently washed with Dulbecco's Phosphate-Buffered Saline (DPBS) (Life Technologies) using 3ml/75 cm^2 flask then DPBS was aspirated and discarded. TrypLE™ Express was added using 3ml/75 cm^2 flask, distributed evenly on cell surface, where cells were incubated for 3-5 minutes at 37°C until cells have detached. Three ml of growth medium were added, where the flask was tilted in all directions to thoroughly rinse flask. Cells suspension was aspirated, transferred to a 15ml Falcon conical tube (BD, Franklin Lakes, USA), and centrifuged for 5 minutes at 300 rpm (Sorvall Legend RT, Thermo Fisher Scientific). The supernatant was discarded and the pelleted cells were re-suspended with 3ml of proliferating medium, with subsequent seeding in 75 cm^2 flask and addition of 7ml of proliferating medium. Flasks were incubated as previously described.

C2C12 murine myoblasts and Hepa-1C1C7 murine hepatoma cells were lysed using Cell Lysis Buffer (Cell Signaling Technology). Briefly, the cell culture flasks were washed with DPBS (Life Technologies) to remove any residual culture media, 400 ul of 1X lysis buffer per flask were added. Flasks were incubated on ice for 5 minutes, cells were scraped, where cells suspension was aspirated and added to microtubes. The extracts were subsequently centrifuged for 10 minutes at 4°C and a speed of 14000 rpm

using Microfuge® 22R Refrigerated Microcentrifuge (Beckman Coulter). The supernatants were collected into new microtubes, whereas the residual pellets were discarded.

Total protein concentrations were determined colourimetrically in a 96-well plate using Pierce BCA ™ Protein Assay Kit (Thermo Fisher Scientific). Optical densities were measured using SpectraMax® 190 Absorbance Microplate Reader and SoftMax Pro Microplate Data Acquisition & Analysis Software (Molecular Devices, Sunnyvale, USA).

3.4 SDS-PAGE and Western Blotting

3.4.1 Sample Preparation

Protein samples were prepared at the appropriate concentration using the NuPAGE® LDS Sample Buffer (4X) and NuPAGE® Sample Reducing Agent (10X) (Life Technologies) at a final concentration of 1X. Samples were heated for 5 minutes at 100°C using VWR® Standard Heat Block (VWR International LLC, Edmonton, Canada), afterwards samples were set to cool down to room temperature and were centrifuged for 1 minute at 1000 rpm using Microfuge® 22R Refrigerated Microcentrifuge (Beckman Coulter).

3.4.2 Electrophoresis

SDS-PAGE was carried out using 1X NuPAGE® MOPS SDS Running Buffer or 1X NuPAGE® Tris-Acetate SDS Running Buffer, NuPAGE® Novex® 4-12% Bis-Tris Mini Gels (1.5 mm) or NuPAGE® Novex® Tris-Acetate Mini Gels (1.5 mm) and XCell SureLock® Mini-Cell Electrophoresis System (Life Technologies). Samples were loaded at the desired protein concentration into each well of the gel, where 10 µl of PageRuler™ Prestained Protein Ladder (Life Technologies) were loaded into one of the wells. Electrophoresis was performed at 200 V constant for 60 minutes.

3.4.3 Preparing for Transfer

Transfer was carried out using 1X NuPAGE® Transfer Buffer and the XCell II™ Blot Module (Life Technologies). Gel/Membrane sandwiches were prepared using Immobilon®-P PVDF; polyvinylidene difluoride membranes, (Millipore, EMD Millipore, Billerica, USA) pre-wetted for 30 seconds in methanol, as well as sponge pads for blotting (Life Technologies) and grade GB005 Whatman® gel blotting papers, both thoroughly presoaked in 1X NuPAGE® Transfer Buffer. The sandwiches were placed in the Blot Module, which was filled with the Transfer Buffer until the sandwich is covered, while the Outer Buffer Chamber was filled with 650 ml deionized water. Transfer was performed at 30 V constant for 120 minutes. Equal protein loading on each gel and equivalent amount of protein transferred to the PVDF membrane was checked using Coomassie blue and Ponceau S staining respectively.

3.4.4 Western Immunodetection

Membranes were taken out of the Blot Module after the transfer completion and placed into incubation/blotting trays on a rocker. Membranes were washed at room temperature for 5 minutes with 10 ml Tris-Buffered Saline with 0.05% Tween 20; TBS-T, prior to blocking at room temperature for 1 hour with 10 ml Bovine Lacto Transfer Technique Optimizer (BLOTTO) composed of TBS-T with 5% skim powder milk (EMD Chemicals Inc., Gibbstown, USA). BLOTTO was decanted then membranes were washed with 10 ml TBS-T twice for 10 minutes and twice for 5 minutes. Membranes were incubated at 4°C overnight with 10 ml primary antibody solution in BLOTTO, afterwards the antibody solution was decanted then membranes were washed as previously described. Membranes were incubated at room temperature for 1 hour with 10 ml secondary antibody solution in BLOTTO, afterwards the antibody solution was decanted then membranes were washed as previously described.

3.4.5 Chemiluminescent Detection

Immunoreactive bands were detected by Thermo Scientific SuperSignal® West Femto Substrate (Thermo Fisher Scientific) using 100 ul developing solution per 1 cm^2 membrane. Any excess solution was drained off the membranes using Kimwipes® (VWR*)*, where the membranes were placed between 2 sheets of transparency plastic ready for imaging. Images were captured using CHEMI GENIUS^2, Gene Snap 6.05 Image Acquisition Software (SynGene, Frederick, USA) and the densitometric analysis was performed on bands using GeneTools 3.06 (SynGene).

Following quantification of each phosphorylated protein, the membrane was stripped by incubating the membrane for 15 minutes in 10ml of 1X ReBlot Plus Strong Antibody Stripping Solution (10X) (EMD Millipore, Billerica, USA) where the stripping solution was decanted then membranes were washed as previously described. As formerly explained, membranes were blocked, washed and further incubated with the specific corresponding antibodies to determine total protein content of each protein.

The densitometric data were expressed in arbitrary units by normalizing phosphorylated proteins to total protein abundance. Alpha-smooth muscle Actin (Sigma-Aldrich) was used as loading control.

3.5 Quantitative Reverse Transcription Polymerase Chain Reaction

The relative expression of hexokinase 2 (*HK2*), solute carrier family 4 (*SLC2A4*) a.k.a glucose transporter type 4 (*GLUT4*), solute carrier family 1 (*SLC2A1*) a.k.a glucose transporter type 1 (*GLUT1*), glycogenin 1 (*GYG1*), and interleukin 6 (*IL*-6) were determined by quantitative reverse transcription PCR (qRT-PCR) using the Bio-Rad C1000 Thermal Cycler (Bio-Rad Laboratories Inc., Hercules, USA).

RNA was isolated from frozen gastrocnemius muscle and liver tissues using TRIzol® Reagent (Life Technologies) using standard phenol/chloroform extraction and 2-propanol precipitation techniques. RNA quality and concentration were determined using the Thermo Scientific NanoDrop™ 2000 Spectrophotometer (Thermo Fischer Scientific) following the manufacturer's instructions. First-strand cDNA was generated from 0.9 ug total RNA using the High Capacity RNA-to-cDNA kit (Life Technologies).

OligoPerfect™ Designer Software (Life Technologies) was used to design primers as described in (Table 3-1**)**. qRT-PCR was performed in triplicates with reaction volumes of 23 ul, containing iQ™SyBR® Green Supermix (Bio-Rad), forward and reverse primers, DEPC-treated water and cDNA template (diluted 1:20). The relative amounts of RNA were calculated using the C_T method. To compensate for variations in input RNA amounts and efficiency of reverse transcription, alpha smooth muscle Actin mRNA was quantified and used for normalization of values.

Table 3-1: Primer sequences used in qRT-PCR.

Gene Name	**Primers**	**Primer Sequence**
HK2	Sense	5'-AACCTCAAAGTGACGGTGGG-3'
	Antisense	5'-TCACATTTCGGAGCCAGATCT-3'
GLUT4 (SLC2A4)	Sense	5'-GTGACTGGAACACTGGTCCTA-3'
	Antisense	5'-CCAGCCACGTTGCATTGTAG-3'
GLUT1 (SLC2A1)	Sense	5'- CTCTGTCGGGGGGCATGATTG-3'
	Antisense	5'-TTGGAGAAGCCCATAAGCACA-3'
GYG1	Sense	5'- CTCACCAGCCCACAGGTTTC-3'
	Antisense	5'-GAGCAGAATCACCACTGTCCAA-3'
IL-6	Sense	5'-AGAAGGAGTGGCTAAGGACCAA-3'
	Antisense	5'-AACGCACTAGGTTTGCCGAG-3'

3.6 Measurement of Glycogen Content

Glycogen concentration in gastrocnemius muscle and liver was determined colourimetrically using BioVision® Glycogen Assay Kit (BioVision Inc., Mountain View, USA). In the assay, glucoamylase enzyme (amyloglucosidase; γ-Amylase; 1,4-α-D-glucan glucohydrolase) hydrolyzes glycogen into glucose which is specifically oxidized to produce a product that reacts with OxiRed probe to generate a colour at λmax = 570 nm. The assay is suitable to detect glycogen between 0.0004 and 2 mg/ml.

Glycogen concentration in tissues was determined following the manufacturer instructions. Briefly, the Glycogen Standard (MW ≈ 10^6-10^7daltons) was diluted to 0.2 mg/ml, mixed well, added into a series of wells in a 96-well plate, where the volume was adjusted up with Hydrolysis Buffer to generate 0, 0.4, 0.8, 1.2, 1.6 and 2.0 µg per well of the Glycogen Standard.

Tissues were homogenized with ultrapure water on ice, where the homogenates were boiled for 5 minutes to inactivate enzymes. The boiled samples were centrifuged for 5 minutes at 13000 rpm Microfuge® 22R Refrigerated Microcentrifuge, (Beckman Coulter), collecting the supernatant for assay, discarding the pellet. Enzyme Mix was added to the wells of standards and test samples, mixed well, incubated for 30 minutes at room temperature. Reaction Mix was prepared by adding Development Buffer, Development Enzyme Mix, and OxiRed Probe, then added standard or samples and incubated at room temperature for 30 minutes, protected from light. The absorbance of the resulting colour was measured at λmax = 570 nm.

Potential background was corrected by subtracting the zero-glycogen control from all sample readings. The standard curve was plotted as μg/well vs. standard readings. Sample readings were applied to the standard curve to get the glycogen concentration in the sample wells according to the following equation: C = Ay/Sv (μg/μl, or mg/ml), where: C is the glycogen concentration in the test samples, Ay is the amount of glycogen (μg) in the sample from the standard curve and Sv is the sample volume (μl) added to the sample well.

3.7 Measurement of Lactate Levels

Lactate level in blood was determined colourimetrically using BioVision® Lactate Assay Kit (BioVision Inc., Mountain View, USA). In the assay, lactate specifically reacts with an enzyme mix to generate a product, which interacts with a lactate probe to produce a color at λmax = 570 nm. The assay is suitable to detect 0.001-10 mM of various lactate samples.

Lactate levels were determined following the manufacturer instructions. Briefly, the Lactate Standard (MW= 90.08) was diluted to 1 nmol/μl, mixed well, added into a series of wells in a 96-well plate, where the volume was adjusted with Lactate Assay Buffer to generate 0, 2, 4, 6, 8, 10 nmol/well of the L(+)- Lactate Standard. Test samples were prepared in with Lactate Assay Buffer in the 96-well plate. Reaction Mix was prepared by adding Lactate Assay Buffer, Enzyme Mix, Probe, then added to wells of standard or test samples, incubated at room temperature for 30 minutes, and protected from light.

Potential background was corrected by subtracting the zero-lactate control from all sample readings. The standard curve was plotted as nmol/well vs. standard readings. Sample readings were applied to the standard curve to get the amount of lactate in the sample wells according to the following equation: C = La/Sv (nmol/µl or mM), where: C is the lactate concentration in the test samples, La is the lactic acid amount (nmol) of the sample from standard curve, Sv is the sample volume (µl) added into the well.

3.8 [3H]-2- deoxy-D-glucose Uptake Assay

Differentiated C2C12 skeletal muscle cells (myotubes) grown in 24-well plates were washed three times with 1X PBS (Life Technologies) prior to incubation for 2 hours in serum-free Ham's F12 nutrient mixture (Life Technologies) containing 0.5% Penicillin Streptomycin and 0.5% Amphotericin B [10000 Unit Penicillin, 10 mg Streptomycin, 25 ug Amphotericin B per ml] (Sigma-Aldrich) in the absence or presence of recombinant MSTN (100ug/ml) for one hour. Cells were washed a further three times with 1X PBS.

Cells were then incubated in pre-warmed cell buffer (2 mM sodium pyruvate ($C_3H_3NaO_3$), 2% BSA, 125 mM NaCl, 5 mM KCl, 1.8 mM $CaCl_2$, 2.6 mM $MgSO_4$, 25 mM HEPES; pH 7.4) then exposed to 100 nM recombinant human insulin (Sigma-Aldrich) for 10 minutes at 37ºC. The uptake of glucose was assayed as previously described (Hundal, Bilan et al. 1994), briefly, by incubating cells with [3H]-2-deoxy-D-glucose (1 µCi/ml) for 20 minutes. Glucose uptake was determined by rapidly aspirating the radioactive medium, followed by 4 successive washes in ice-cold 1X PBS. Cells were lysed using 0.5% SDS (Sigma-Aldrich) and the associated radioactivity was determined

using Liquid Scintillation Analyzer Tri-Carb® 2800TR (PerkinElmer Life and Analytical Sciences, Shelton, USA). Total cell protein was determined using the Pierce BCA ™ Protein Assay Kit (Thermo Fisher Scientific).

3.9 High-Resolution Respirometry

All protocols used in the high-resolution respirometry assessments were executed following the instructions of OROBOROS® Instruments as described in OROBOROS Protocols (MiPNet08.09_CellRespiration) and Oxygraph-2k Manual (MiPNet12.09_O2FluxAnalysis). Chemicals were used for the preparation of titrants (both inhibitors and uncouplers) according to instructions, recipes and concentrations describes in Oxygraph-2k Manual (MiPNet03.02_Chemicals-Media).

3.9.1 Mitochondrial Respiration

Mitochondrial performance of skeletal muscle and liver cells was assessed using high-resolution respirometry OROBOROS Oxygraph-2k; O2k (OROBOROS® Instruments, Innsbruck, Austria). Confluent myoblasts were differentiated for 3 days (72 hours); afterwards, the differentiating myotubes were further differentiated for 72 hours in the absence or presence of recombinant MSTN (10 μg/ml). Liver cells were grown to 90% confluence, where the test group received recombinant MSTN (1.5 μg/ml, one hour), while the control group received no treatment (Chen, Ye et al. 2010). Myotubes or liver cells were trypsinized, as previously described under cell culture, where the wet weight of the pellet was determined using Mettler HK160 Analytical Balance (Thermo

Fisher Scientific). The optimization of the minimal wet weights of trypsinized myotubes or liver cells to be used for respirometry experiments were achieved as follows: a series of the wet weights of untreated trypsinized cells, ranging from 5 mg to 75 mg with a 5 mg-increment, was run –separately- in the O-2k with the addition of various titrants as described below under phosphorylation control protocol (PCP). The minimal wet weights that could be detected by the polarographic oxygen sensors (POS) inducing an oxygen flux and also complete the entire PCP without early oxygen depletion in the chambers were chosen for every type of cells. Each experiment was conducted as a single run in duplicates; using both chambers of the oxygraph in parallel. Experiments were repeated three times for both control and test groups.

3.9.2 Phosphorylation Control Protocol

O-2k is designed to operate at 37.0 °C using 2 ml of total volume in both respiratory chambers. Using polyether ether ketone (PEEK) stirrers, O-2k provides an adjustable stirring velocity that was maintained at 750 rpm in every chamber. Prior to the assessment of cellular respiration, POS were calibrated where the instrumental background controls were determined and used for instrumental calibration (MiPNet12.09_O2FluxAnalysis). The stoppers were kept partially opened for 60 minutes to allow the respiratory medium, DMEM, to be fully oxygenated by atmospheric air diffusing into the chambers and to ensure signal stabilization. The cell suspensions of trypsinized myotubes or liver cells in DMEM were pipetted, using an automatic pipette, into the chambers at a concentration of 12.5 mg wet weight/ml and 25 mg wet weight/ml

respectively, using glucose - available in DMEM - as a primary substrate for mitochondrial respiration. The rotating stirrers guaranteed a homogenous distribution of the sample throughout the chamber. The stoppers were kept partially opened for few minutes to allow for the stabilization of oxygen flux signal. Afterwards, the chambers were tightly closed and the oxygen flux signal was allowed to run for 10-15 minutes to assess ROUTINE respiration (State R). Titrants were added into the chambers using a Hamilton syringe (Sigma-Aldrich), where successive injections (1 µl) of ethanol solutions of oligomycin (5 µM/chamber) (Sigma-Aldrich) were added till oxygen flux reached the lowest possible flux. Minimum oxygen flux was determined when a subsequent injection of oligomycin caused no further reduction in oxygen flux where flux starts to increase despite the addition of oligomycin. Oxygen flux signal was allowed to run for 5 minutes to assess LEAK respiration (State L). Then, successive injections (2 µl) of ethanol solutions of FCCP (2 µM/chamber) (Sigma-Aldrich) were added till oxygen flux reached the highest possible flux in order to assess Electron Transport System (ETS, E). Maximum oxygen flux was determined when a subsequent injection of FCCP caused a reduction in oxygen flux due to inhibition of ETS by excess FCCP. All titrants used in PCP are readily permeable across the intact cell membrane, making it unnecessary to permeabilize the cell membrane. After completing PCP, oxygen flux sections; R, L, E; are marked to calculate the average oxygen flux for State R and State L. Respiratory flux per volume (pmol/s.ml) was converted to a mass-specific quantity (pmol/s.mg) after being normalized to wet mass of samples (mg). Mass-specific fluxes were further normalized to the mitochondrial marker Cytochrome c oxidase; Complex IV (COX IV).

The phosphorylation control protocol (PCP) assesses: (1) Cellular ROUTINE respiration (State R); which is the aerobic metabolic activity under routine culture conditions, (2) Oligomycin-inhibited LEAK respiration (State L, State 4), which is due to the compensatory proton leak in response to ATP synthase inhibition (Complex V) and (3) FCCP-stimulated respiration, which is the electron transfer system (ETS) capacity at non-coupled respiration of intact cells (State E, State 3u) where FCCP; carbonylcyanide-p-trifluoromethoxyphenylhydrazone functions as a protonophore therefore dissipating mitochondrial membrane potential thus activating ETS to its maximum capacity.

In addition to the previous absolute respiratory fluxes, PCP provides information about flux control ratios (FCR), particularly ROUTINE and LEAK flux control ratios. FCRs are ratios of oxygen flux in various respiratory control states, being normalized for maximum flux in a common reference state, thus obtaining theoretical minimum and maximum thresholds of 0 and 1 i.e. 0% and 100%. FCRs obtained from the same respirometric incubation using a sequential protocol such as PCP provide internal normalization, therefore, offering the advantage of expressing respiratory control independent of the amount of mitochondria and also independent of a marker for mitochondrial content.

ROUTINE flux control ratio, (R/E), is the ratio of coupled ROUTINE respiration (R) to non-coupled ETS capacity (E). It is an expression of how close ROUTINE respiration operates compared to the respiratory capacity of the ETS. LEAK flux control ratio, (L/E), is the ratio of non-coupled LEAK respiration (L) and non-coupled ETS capacity (E). It is an index of the degree of uncoupling at constant ETS capacity. L/E increases in magnitude as uncoupling increases, from a theoretical minimum of 0 for a fully coupled

system to a maximum of 1 for a fully uncoupled/non-coupled system. In intact cells, (R/E) and (L/E) are also referred to as coupling control ratios (CCR).

The reciprocal ratio, (E/L), is the respiratory control ratio, (RCR), which is an index of the functional integrity of prepared mitochondria where it is of higher magnitude in good mitochondrial preparations.

3.10 Statistical Analysis

All data were expressed as mean ± standard error of the mean (SEM). Two-tailed students *t* tests were performed on data at a minimum $p < 0.05$ threshold.

Chapter Four: **RESULTS**

4.1 Investigation of the role of myostatin in glucose metabolism and insulin sensitivity *in vivo* and *in vitro*

4.1.1 Body Weight and Muscle Weight

Mice treated for 5 days with IP injection (2ug/mouse/day) of recombinant MSTN (MSTN) showed no significant change (p= 0.15, p=0.82, p=0.48 for day "1", "2" and "5" respectively) in their body weights compared to PBS-treated mice (CTRL). The isolated gastrocnemius muscles, collected on day "6", showed no significant difference (p=0.47, p=0.56 for right and left gastrocnemius respectively) upon MSTN treatment, compared to CTRL group. All values represent the mean ± SEM for PBS- (white bars, n=6) and MSTN-treated (black bars, n=6) male mice (Table 4-1).

Table4-1: Characteristics of PBS- (CTRL) and MSTN-treated (MSTN) mice.

Weight		CTRL (n=6)	MSTN (n=6)
Body (g)	Day 1	22.02±0.39	22.72±0.22
	Day 2	22.43±0.45	22.32±0.22
	Day 5	22.68±0.68	22.32±0.55
Gastrocnemius Muscle (mg)	Right	146.65±8.25	139.93±3.19
	Left	146.67±8.21	141.42±3.03

4.1.2 Glucose Tolerance Test

On the fifth day of treatment, the glycaemic response of the PBS- and MSTN-treated mice was measured via an IP GTT, following a four-hour fast (Figure 4-1 **A, B**). Results demonstrate the mean BGL over a two-hour period. Total area under the curve (AUC) for each GTT line graph was calculated using the trapezoidal method. There were no significant differences (p=0.25) in BGL between the PBS- and MSTN-treated groups (CTRL and MSTN respectively) at any of the time points over the two hours or after calculating AUC. However, there was a trend towards a decreased AUC in MSTN-treated mice, suggesting an increased glucose uptake.

Interestingly, this trend, although statistically non-significant, comes in accordance with previous unpublished observations from our lab (Figure 4-1 **C, D**) which showed significant increase in glucose uptake upon MSTN-treatment. All values represent the mean ± SEM for PBS- (white squares or bar, n=6) and MSTN-treated (black squares or bar, n=6) male mice.

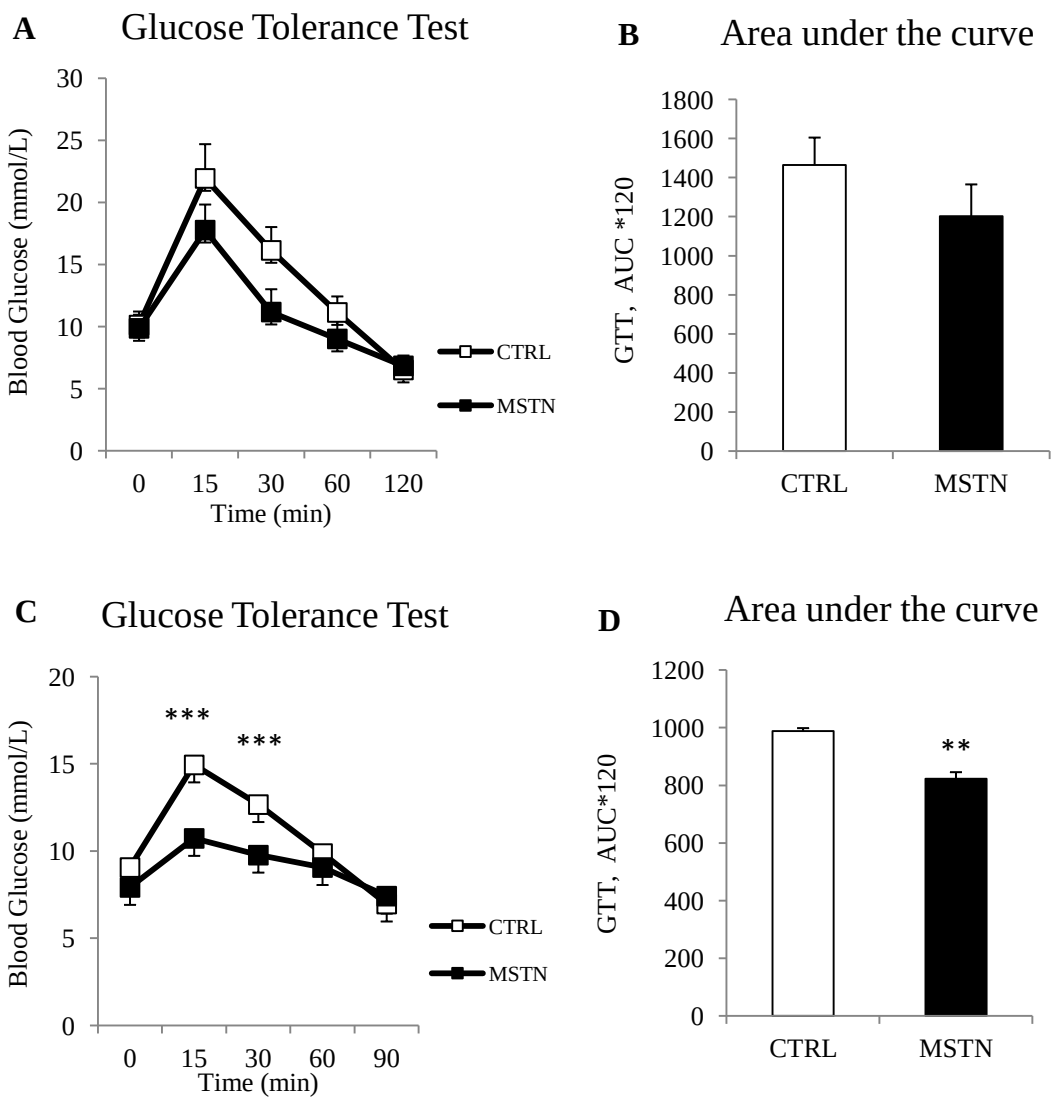

Figure 4-1: Glucose tolerance test (GTT) in mice.

(A, C): Blood glucose levels (BGL) after the initial administration of glucose, **(B, D):** Areas under the glucose curve (AUC) for both PBS- and MSTN-treated mice (CTRL and MSTN respectively). All values represent the mean ± SEM for PBS- (white squares or bar, n=6) and MSTN-treated (black squares or bar, n=6) mice. (**) and (***) denote $p < 0.01$ and $p < 0.001$ respectively for each time point for PBS- versus MSTN-treated mice.

4.1.3 Insulin Tolerance Test

On the sixth day, the glycaemic response of the PBS- and MSTN-treated mice was measured via an IP ITT, following a four-hour fast (Figure 4-2 **A, B**). Results demonstrate the mean BGL over a two-hour period. Total AUC for each ITT line graph was calculated using the trapezoidal method. BGL at the time point at "15 minutes" was significantly higher (p=0.043) in the MSTN-treated groups compared to CTRL group, while AUC showed no significant difference between the two groups (p=0.25). Interestingly, the magnitude of MSTN-induced changes in ITT was similar to but *less* than previously reported by Hittel et al (Figure 4-2 **C, D**), who described induction of IR upon short-term MSTN administration (Hittel, Axelson et al. 2010). All values represent the mean ± SEM for PBS- (white squares or bar, n=6) and MSTN-treated (black squares or bar, n=6) male mice.

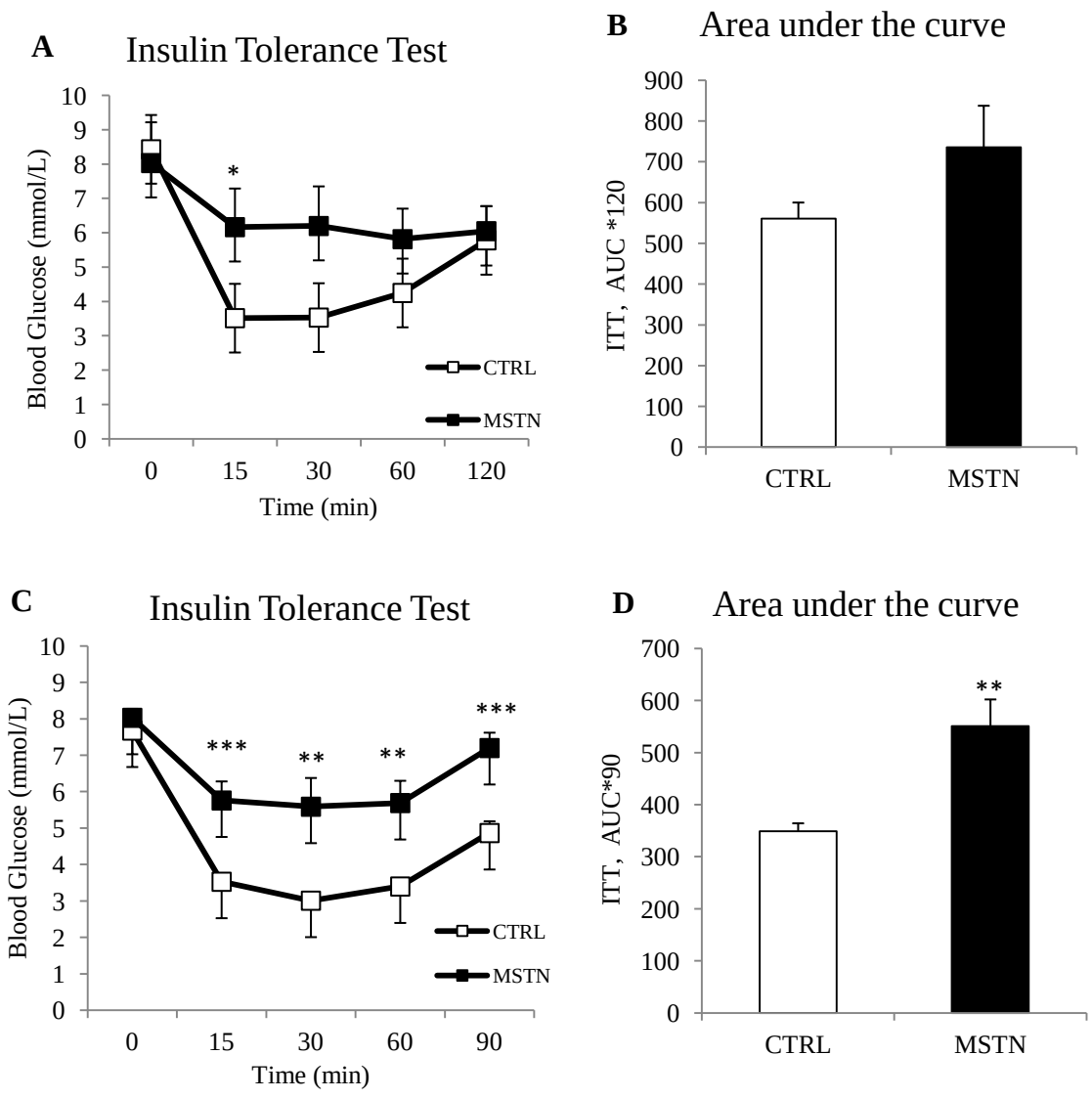

Figure 4-2: Insulin tolerance test (ITT) in mice.

(A, C): Blood glucose levels (BGL) after the initial administration of insulin, **(B, D):** Areas under the glucose curve (AUC) for both PBS- and MSTN-treated mice (CTRL and MSTN respectively). All values represent the mean ± SEM for PBS- (white squares or bar, n=6) and MSTN-treated (black squares or bar, n=6) mice. (*), (**) and (***) denote

$p < 0.05$, $p < 0.01$ and $p < 0.001$ respectively for each time point for PBS- versus MSTN-treated mice.

4.1.4 Glycogen Content of Muscle and Liver

Results **(**Figure 4-3**)** represent the mean glycogen content (ug glycogen/mg wet mass of tissue) in skeletal muscle **(A)** and in liver **(B)**. MSTN-treatment (MSTN) showed a significant decrease in hepatic glycogen content (p=0.03) compared to PBS-treated group (CTRL), whereas there was no significant change in muscle glycogen content (p=0.22) between the two groups. All values represent the mean ± SEM for PBS- (white bars, n=10) and MSTN-treated (black bars, n=10) male mice.

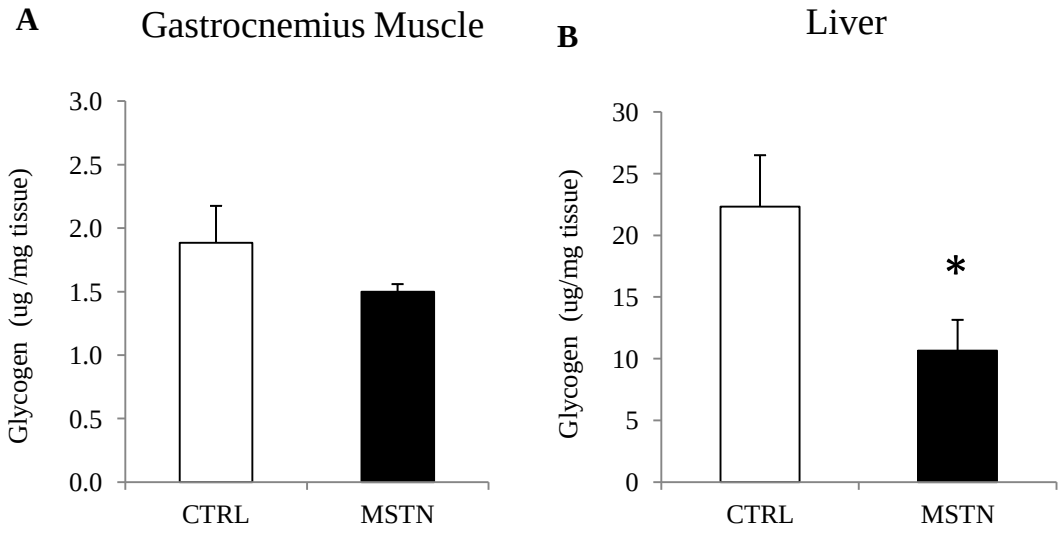

Figure 4-3: Glycogen content in skeletal muscle and liver of mice.

Glycogen content (ug glycogen/mg wet weight of tissue) was measured in gastrocnemius muscle **(A)** and liver **(B)** in PBS- and MSTN-treated mice (CTRL and MSTN

respectively)**.** All values represent the mean ± SEM for PBS- (white bars, n=10) and MSTN-treated (black bars, n=10) male mice. (*) denotes $p < 0.05$ for PBS- versus MSTN-treated mice.

4.1.5 Blood Lactate Levels

Results (Figure 4-4).represent the mean blood lactate levels (mM); the product of cellular glycolysis. MSTN-treatment showed no significant differences ($p>0.05$) from the CTRL group, suggesting no change in anaerobic glycolysis. All values represent the mean ± SEM for PBS- (white bar, n=10) and MSTN-treated (black bar, n=10) male mice.

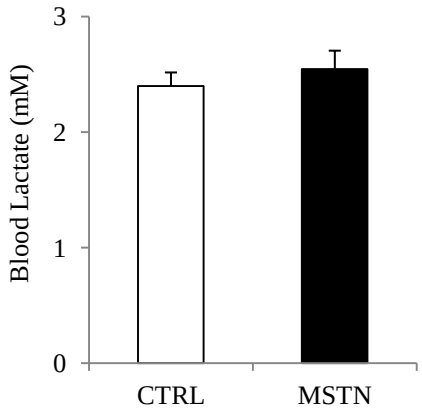

Figure 4-4: Blood lactate level of mice.

Blood lactate levels were measured in PBS- and MSTN-treated mice (CTRL and MSTN respectively). All values represent the mean ± SEM for PBS- (white bar, n=10) and MSTN-treated (black bar, n=10) mice.

4.1.6 qRT-PCR for Glucose Metabolism Genes

To provide a molecular evidence of the MSTN function in the regulation of glucose metabolism, we used quantitative reverse transcription polymerase chain reaction (qRT-PCR) to validate five genes involved in glucose metabolism, reported (Chen, Ye et al. 2010) to be responsive to MSTN treatment.(Figure 4-5). The expression levels of the genes in gastrocnemius muscle **(A)** and liver **(B)** showed no significant difference (p>0.05) in any of the five genes between the PBS- and MSTN-treated mice. However, gastrocnemius muscle showed a tendency towards a significant reduction in the genes related to glucose transport (*GLUT1*) and glycogen synthesis (*GYG1*) with a *p*-value of 0.053 and 0.056 respectively. All values represent the mean ± SEM for PBS- (white bars, n=6) and MSTN-treated (black bars, n=10) mice.

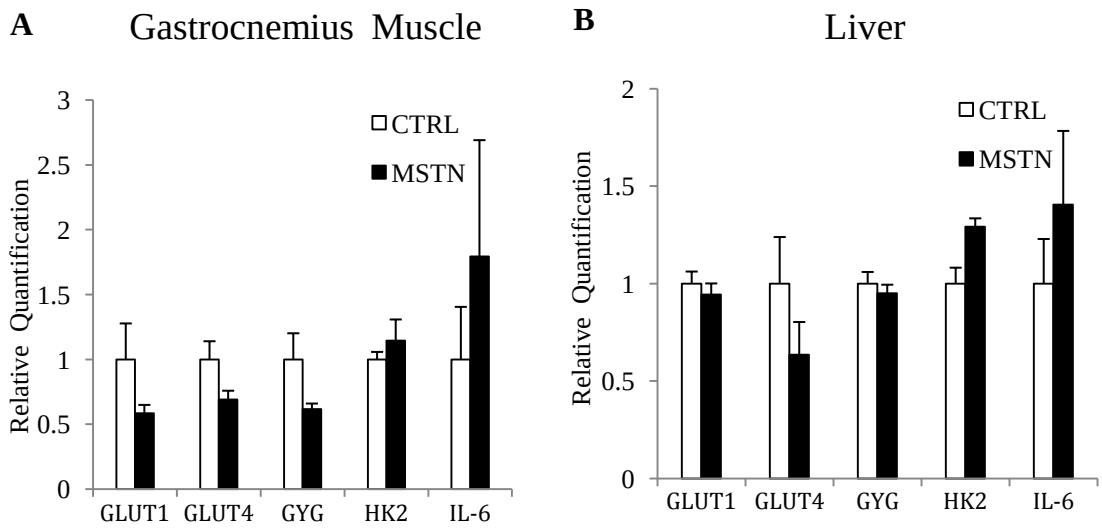

Figure 4-5: qRT-PCR for glucose metabolism genes in skeletal muscle and liver of mice.

Glucose transporter 1 (*GLUT1*), glucose transporter 4 (*GLUT4*), glycogenin (*GYG1*), hexokinase 2 (*HK2*) and interleukin 6 (*IL-6*) gene expression was measured in gastrocnemius muscle (A) and in liver (B) in both PBS- and MSTN-treated mice (CTRL and MSTN respectively). All values represent the mean ± SEM for PBS- (white bars, n=6) and MSTN-treated (black bars, n=10) mice.

4.1.7 [3H]-2-deoxy-D-glucose Uptake (2-DG)

Basal and insulin-stimulated (100nM/ml) glucose uptake was determined *in vitro* (Figure 4-6) in C2C12 **(A)** and liver **(B)** cells in the absence (CTRL) or presence of recombinant MSTN (MSTN) using liquid scintillation counting. After one hour of MSTN (100ug/ml) treatment, C2C12 cells did not show any significant difference in basal or in insulin-stimulated glucose uptake in contrast to Chen *et al*. previous report (Chen, Ye et al. 2010). However, after one hour of MSTN treatment, liver cells showed a significant reduction (p=0.047) in insulin-stimulated glucose uptake in MSTN group compared to CTRL group. Also, liver cells showed significantly higher (p=0.046) insulin-stimulated glucose uptake compared to basal glucose uptake in CTRL group but not in MSTN group. These results reveal that acute MSTN treatment does not increase basal glucose uptake as described previously, on the contrary it decreases insulin-stimulated glucose uptake in a cell-specific manner.

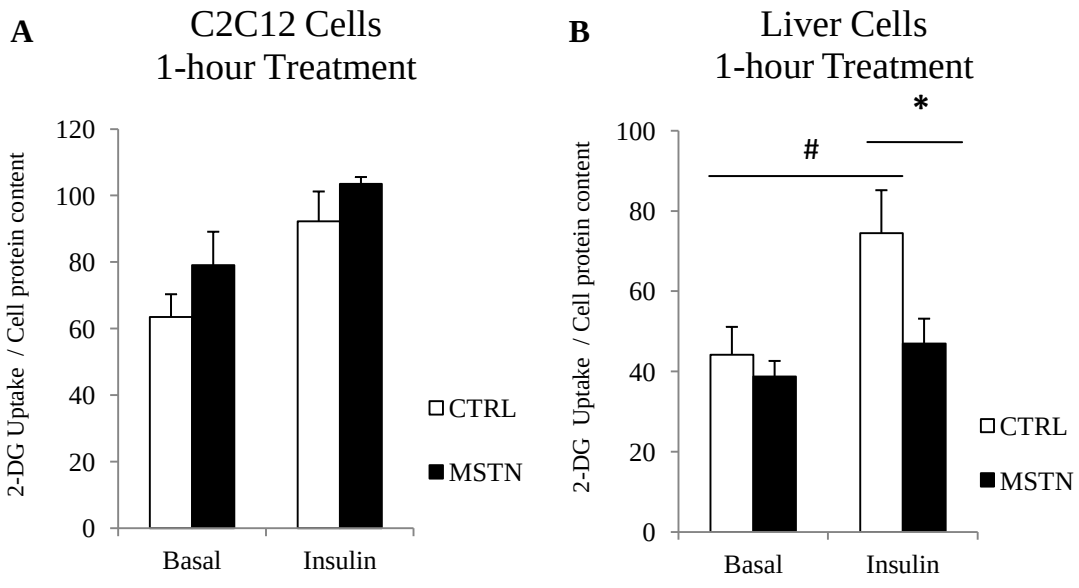

Figure 4-6: [3H]-2-deoxy-D-glucose uptake in skeletal muscle and liver cells.

Basal and insulin-stimulated glucose uptake determined in C2C12 **(A)** and liver **(B)** cells in the absence (CTRL) or presence of MSTN (MSTN). All values represent the mean ± SEM for PBS- (white bars, n=6) and MSTN-treated (black bars, n=6) C2C12 or liver cells. **(*)** denotes significant difference in insulin-stimulated glucose uptake between CTRL and MSTN groups at $p < 0.05$, while **(#)** denotes a significant difference between basal & insulin-stimulated uptake at $p < 0.05$.

4.2 Assessment of the role of AMPK involved in myostatin-regulated glucose metabolism *in vivo* and *in vitro*

4.2.1 Western Blotting

Western blots **(**4-7**)** were carried out to determine the protein expression levels of phosphorylated and AMPKα as well as its target protein; ACC in skeletal muscle **(A, E)** and liver **(B, F).** Densitometric analysis was performed for the western blots where the phosphorylated AMPKα (Thr172) and ACC (Ser79) proteins were normalized to their total protein levels in mice gastrocnemius muscle **(C, G)** and liver **(D, H)**. Neither pAMPK nor pACC showed any significant change (p>0.05) in their protein expression upon MSTN-treatment compared to PBS-treated (CTRL) mice. Similar results were obtained when performing similar western blots (Figure 4-8) in vehicle-treated (CTRL) and MSTN-treated (MSTN) C2C12 myotubes **(I, K)** as well as liver cells **(J, L).** These findings suggest that exogenous recombinant MSTN does not affect AMPK signalling *in vivo* or *in vitro*.

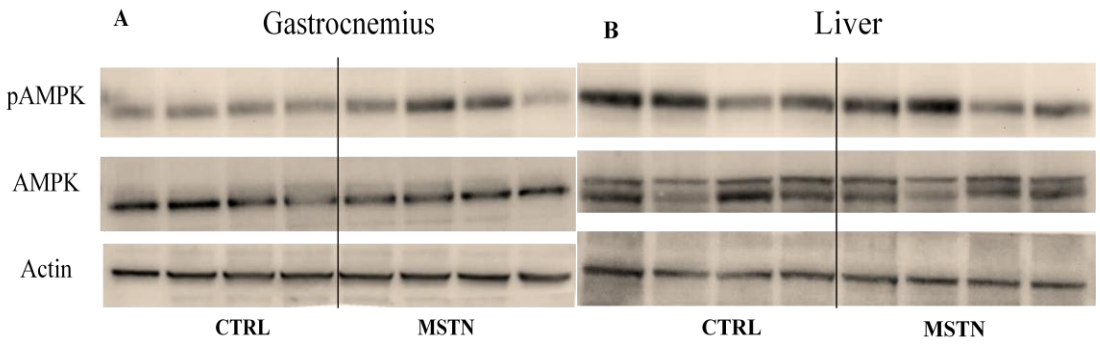
A
Gastrocnemius
B
Liver
pAMPK
AMPK
Actin
CTRL
MSTN
CTRL
MSTN

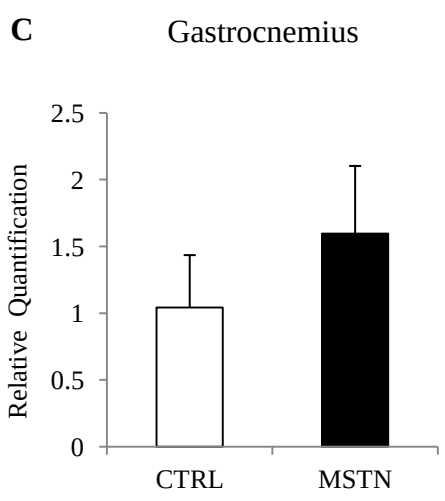
C
Gastrocnemius
Relative Quantification
2.5
2
1.5
1
0.5
0
CTRL
MSTN

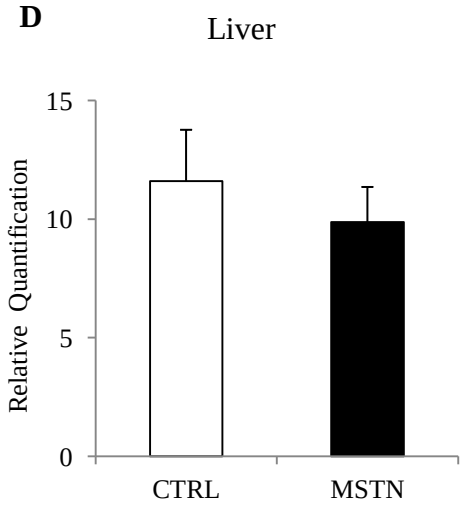
D
Liver
Relative Quantification
15
10
5
0
CTRL
MSTN

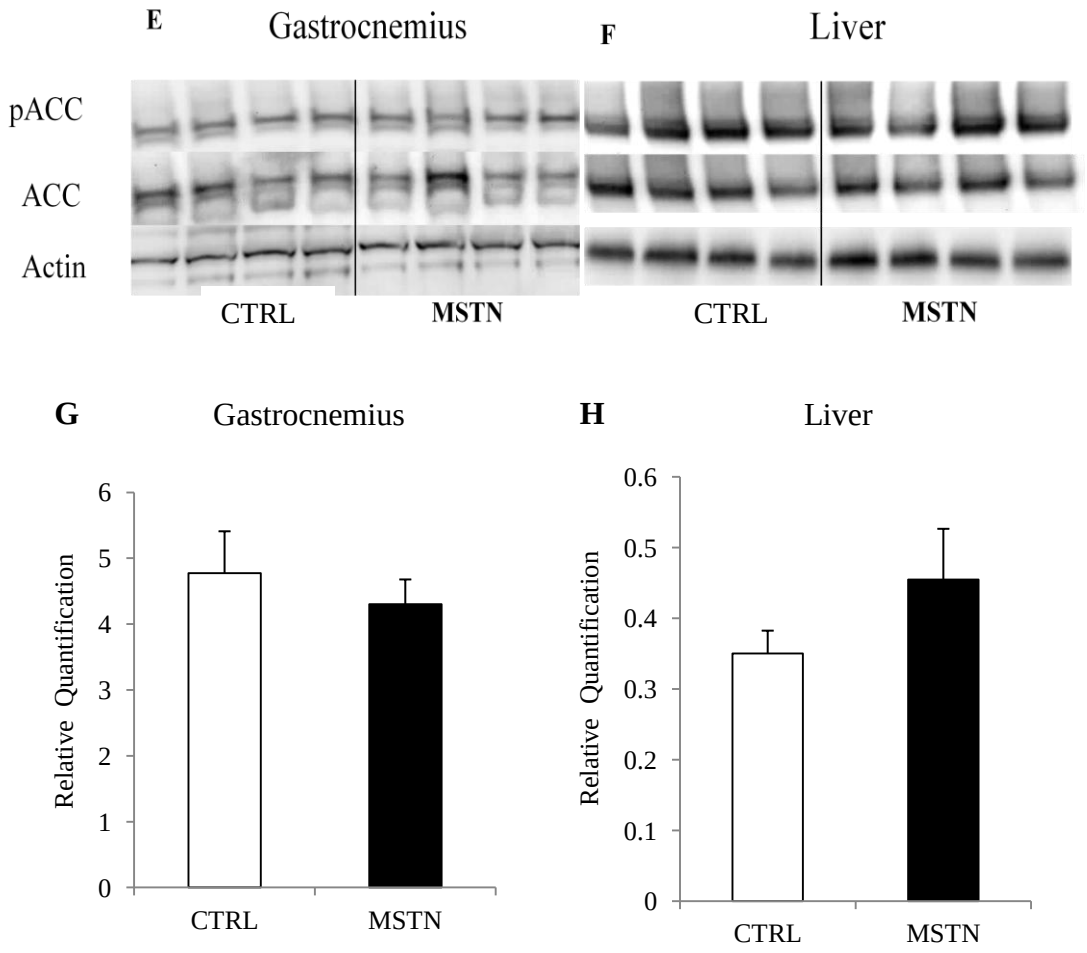

Figure 4-7: Western blots for phosphorylated and total AMPK and ACC in mice.

(A-B) Representative western blots of phosphorylated (Thr172) and total AMPKα in gastrocnemius muscle **(A)** and liver **(B)** of PBS- and MSTN-treated mice (CTRL and MSTN respectively). **(C-D)** Densitometric analysis of phosphorylated AMPKα (Thr172) normalized to total protein levels in gastrocnemius muscle **(C)** and liver **(D)**. **(E-F)** Representative western blots of phosphorylated (Ser79) and total ACC in gastrocnemius muscle **(E)** and liver **(F)**. **(G-H)** Densitometric analysis of phosphorylated ACC (Ser79) normalized total protein levels from gastrocnemius muscle **(G)** and liver **(H)**. Alpha-

smooth muscle Actin was used as loading control. All values represent the mean ± SEM for PBS- (white bars, n=6) and MSTN-treated (black bars, n=6) mice.

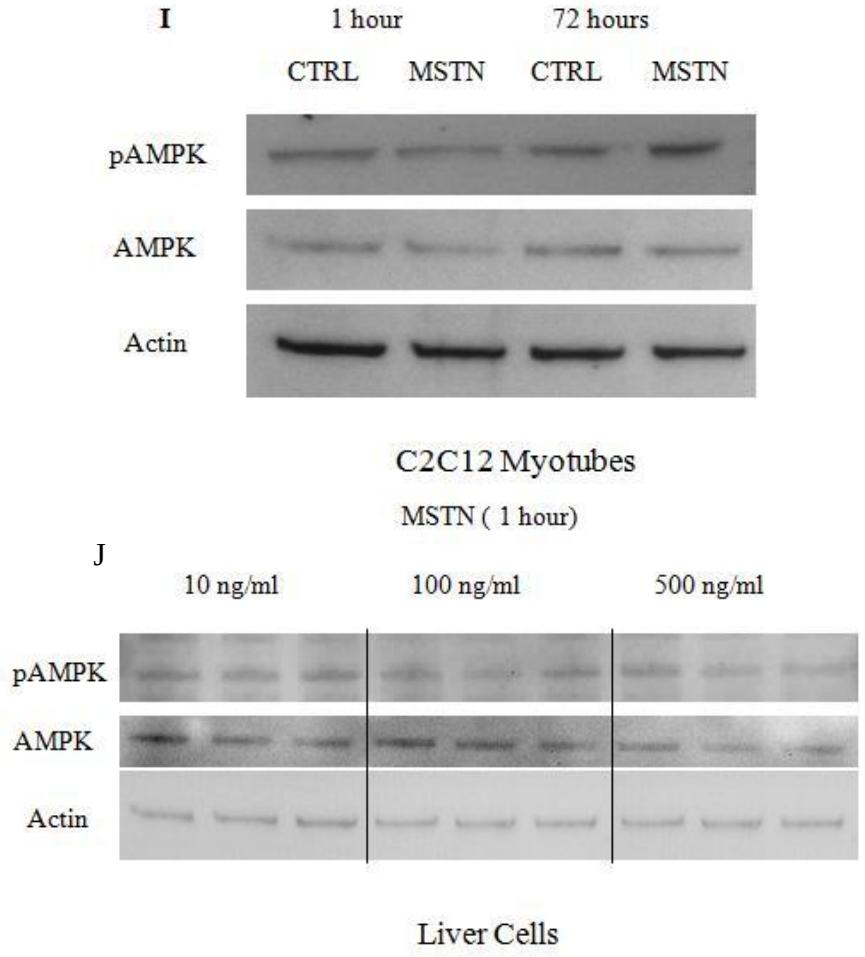

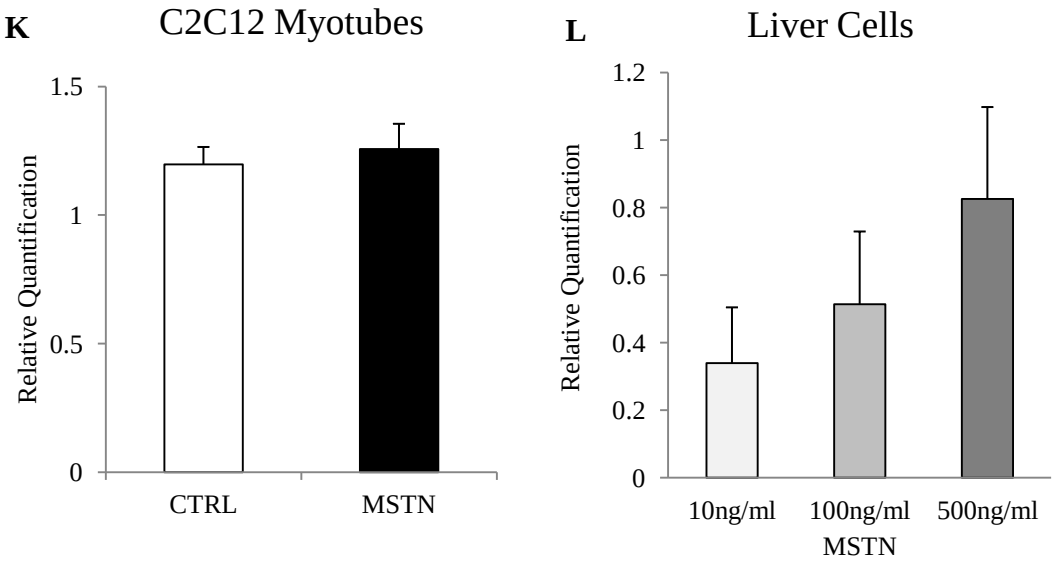

Figure 4-8: Western blots for phosphorylated and total AMPK in myotubes and liver cells.

(I-J) Representative western blots of phosphorylated (Thr172) and total AMPKα from C2C12 myotubes **(I)** and 1C1C7 liver cells **(J)** in the absence and presence of MSTN (CTRL and MSTN respectively)**. (K-L)** Densitometric analysis of phosphorylated AMPKα (Thr172) normalized to total protein levels from myotubes **(K)** and liver cells **(L)**. Alpha-smooth muscle actin was used as loading control. All values represent the mean ± SEM for CTRL (white bars, n=6) and MSTN (grey and black bars, n=6) groups.

4.2.2 Myostatin-Induced Smad2 Phosphorylation

To confirm that MSTN signalling was activated in muscle and liver cells we monitored the activation of its downstream target protein; Smad2 (See Figure 2-1). We were able to show increased levels of phosphorylated Smad2 (S465/467) upon recombinant MSTN treatment (10ug/ml) in C2C12 myoblasts (1 hour), in six-day differentiated C2C12

myotubes (72 hours), and in liver cells (1 hour) compared to CTRL group These findings provide experimental evidence for the activation of the transcription factors Smad2/3 in response to MSTN, thus affecting the downstream effects associated with MSTN signalling, such as glucose metabolism, or AMPK regulation as previously described. (Figure **4-9**)

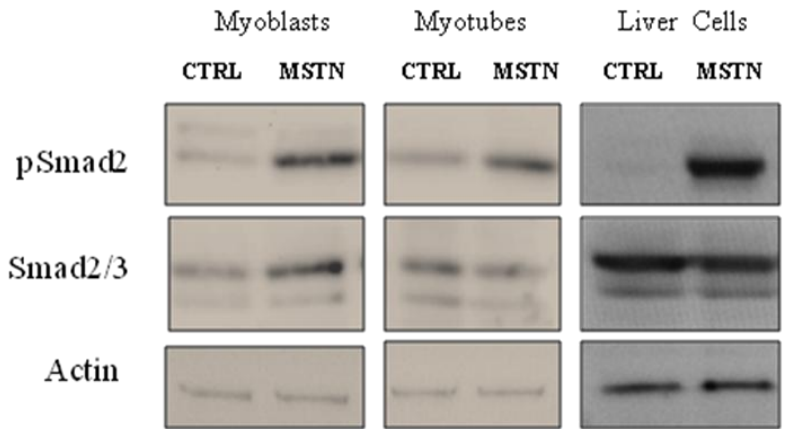

Figure 4-9: Western blots for phosphorylated Smad2 and Smad2/3 in skeletal muscle & liver cells.

Western blots showing the level of phosphorylated Smad2 (S465/467) and Smad2/3 proteins in C2C12 myoblasts, six-day differentiated C2C12 myotubes and in liver cells in CTRL and MSTN groups (n=6). Alpha-smooth muscle actin was used as loading control.

4.3 Evaluation of myostatin effect on glucose-dependent mitochondrial respiration *in vitro* using High-Resolution Respirometry

4.3.1 Myostatin-Induced Atrophy

We adopted an *in vitro* model of MSTN-induced atrophy in C2C12 myotubes to investigate the reported MSTN-induced changes in glucose metabolism and IS; particularly to determine the effect of MSTN on glucose-dependent mitochondrial respiration. Confluent myoblasts were differentiated for 3 days (72 hours) were they fuse together to form myotubes. Afterwards, differentiating myotubes were further differentiated for 3days (72 hours), in the absence or presence of recombinant MSTN (10ug/ml) in CTRL or MSTN groups respectively **(**Figure 4-10**A, B).** The white arrows show thicker, fused, differentiated myotubes in the absence of MSTN (CTRL) **(A),** while the black arrows show thinner, filamentous, less differentiated myotubes in the presence of MSTN (MSTN) **(B).**

Figure 4-10: Myostatin-induced atrophy in six-day differentiated myotubes.

Below: (A, B) Six-day differentiated C2C12 myotubes, in the absence (CTRL) and presence (MSTN) of MSTN (10ug/ml, 72 hours). Differentiated myotubes are indicated by white arrows **(A),** while atrophied myotubes are indicated by black arrows **(B)**.

A

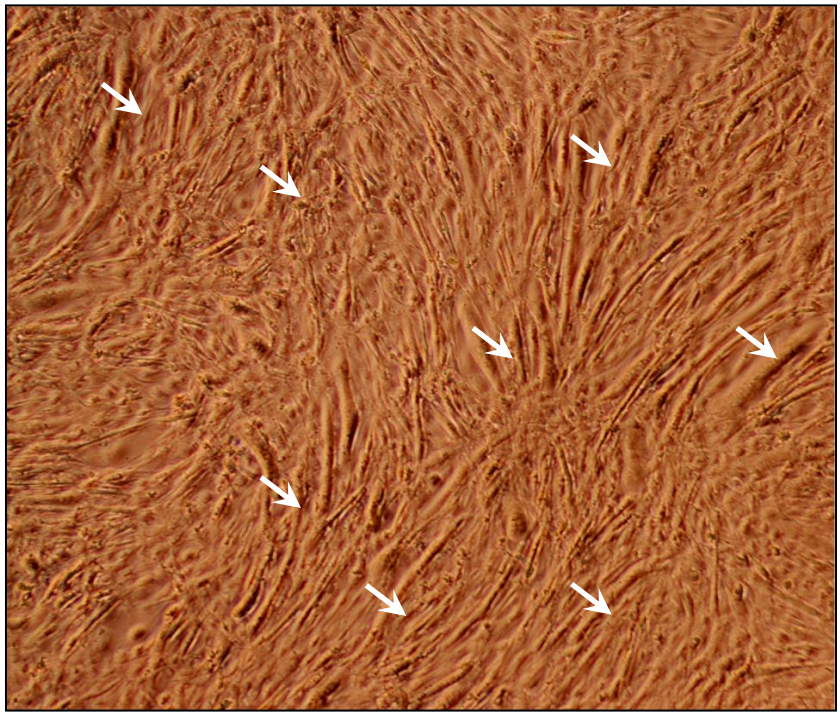

B

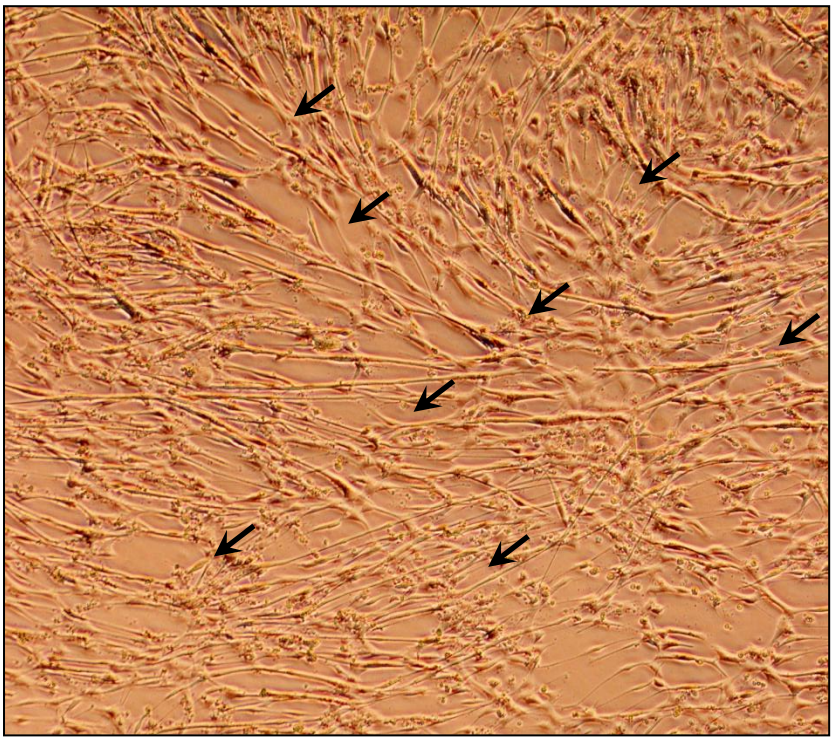

4.3.2 Normalization of Oxygen Fluxes

Mass-specific oxygen fluxes; R, L or E, in myotubes and liver cells were further normalized to their endogenous content of the mitochondrial marker, Cytochrome c oxidase (COX IV).

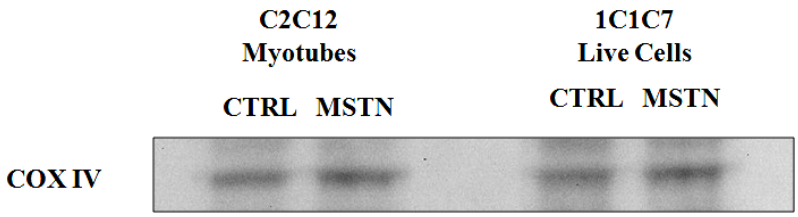

Figure 4-11: Western blots for COX IV in cultured myotubes & liver cells.

Western blots showing the level of the mitochondrial marker COX IV proteins in six-day differentiated C2C12 myotubes (n=6) and in liver cells (n=3) in CTRL and MSTN groups.

4.3.3 Myotubes

4.3.3.1 Mitochondrial Respiratory Capacity

Mass-specific oxygen fluxes; R, L or E showed no significant difference (p>0.05) between CTRL and MSTN groups, thus suggesting a preserved mitochondrial function upon MSTN treatment. All values represent the mean ± SEM for CTRL (white bars, n=8) and MSTN (black bars, n=6) myotubes.

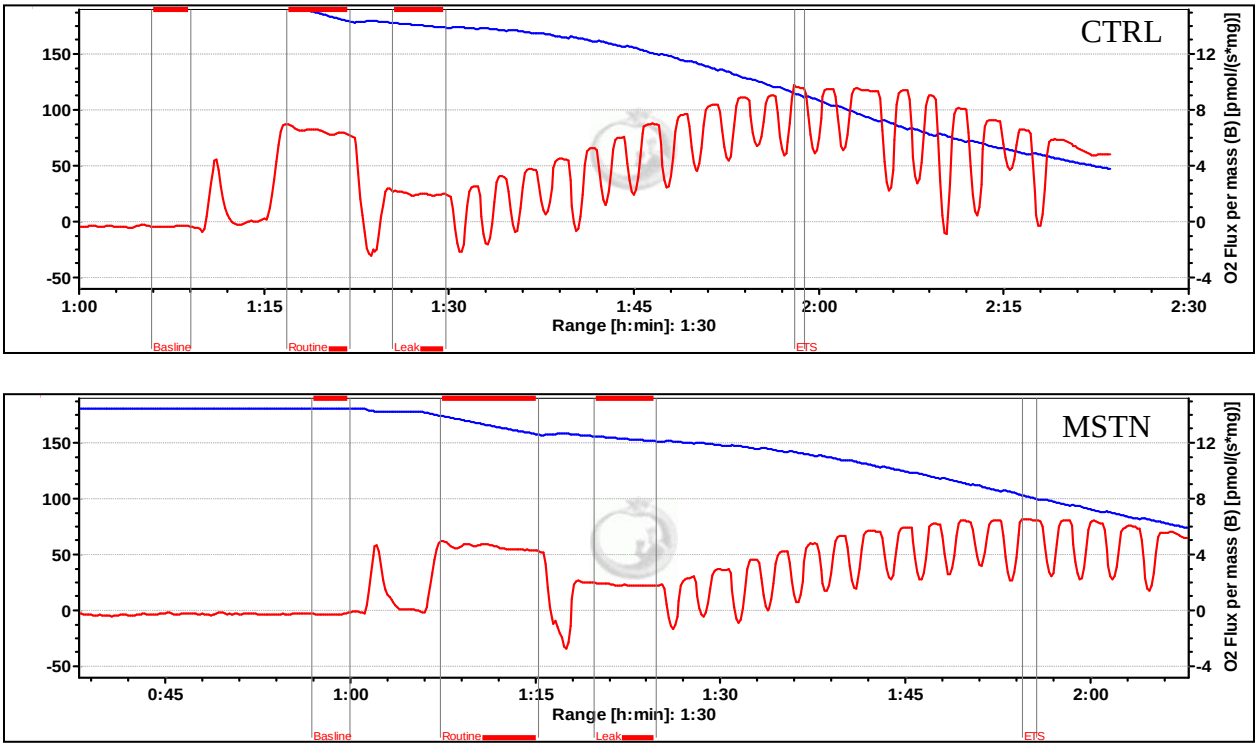

Figure 4-12: Oxygen flux per volume (pmol/s.ml) and oxygen concentration (µM) as a function of time in myotubes.

Representative charts showing oxygen flux per volume (pmol/s.ml) [red lines] and oxygen concentration (µM) [blue lines] corrected for instrumental background as a function of time in untreated (CTRL; top graph) and MSTN-treated (MSTN; bottom graph) myotubes. Marked sections are used to calculate the oxygen flux for R and L states. Baseline represents oxygen flux at full oxygen concentration in O-2k chambers.

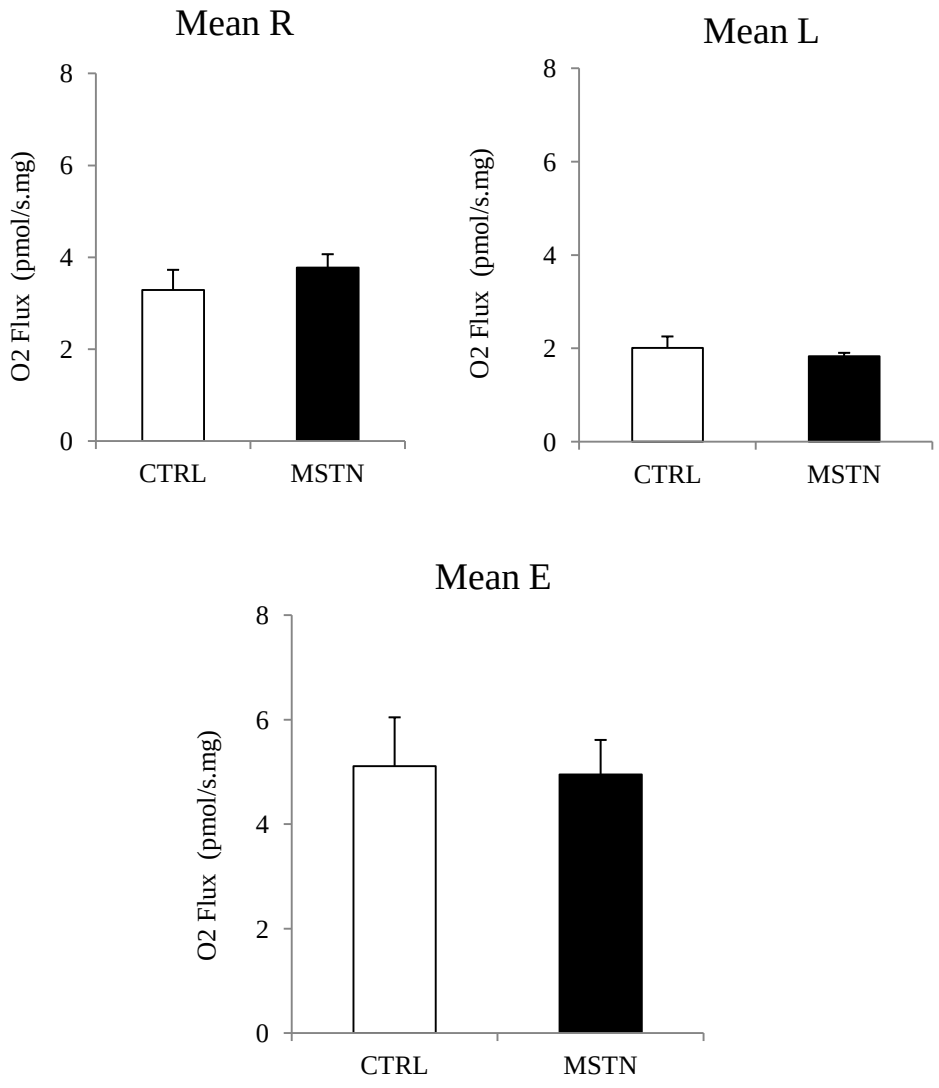

Figure 4-13: Mitochondrial respiratory capacity in myotubes.

Mass-specific oxygen fluxes of Routine (R), Leak (L) and Electron Transport System; ETS (E) respiration were assessed in six-day differentiated C2C12 myotubes in the absence and presence of MSTN (10ug/ml, 72 hours); CTRL and MSTN respectively. All values represent the mean ± SEM for CTRL (white bars, n=8) and MSTN (black bars, n=6) myotubes.

4.3.3.2 Coupling Control Ratios

Flux control ratios of mass-specific oxygen fluxes; (R/E) or (L/E) showed no significant difference (p>0.05) between CTRL and MSTN groups, thus suggesting no change in the coupling tightness of mitochondrial respiration upon MSTN treatment. All values represent the mean ± SEM for CTRL (white bars, n=8) and MSTN (black bars, n=6) myotubes.

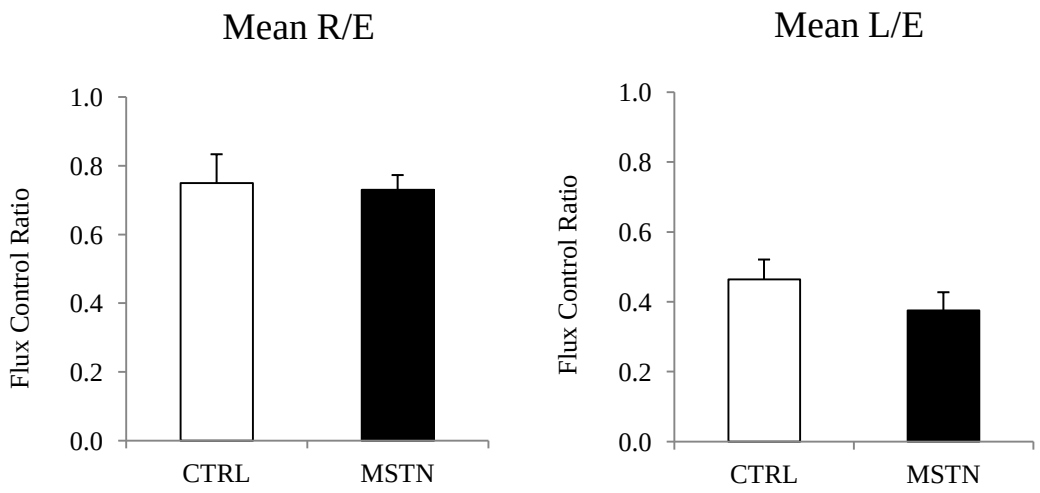

Figure 4-14: Coupling control ratios in myotubes.

Flux control ratios of mass-specific oxygen fluxes for Routine(R) and Leak (L) normalized to Electron Transport System; ETS (E) in six-day differentiated C2C12 myotubes in CTRL and MSTN groups. All values represent the mean ± SEM for CTRL (white bars, n=8) and MSTN (black bars, n=6) myotubes.

4.3.3.3 Respiratory Control Ratio

Respiratory control ratio; (E/L) showed no significant difference (p>0.05) between CTRL and MSTN groups, suggesting no change of mitochondrial integrity upon MSTN treatment. All values represent the mean ± SEM for CTRL (white bars, n=8) and MSTN (black bars, n=6) myotubes.

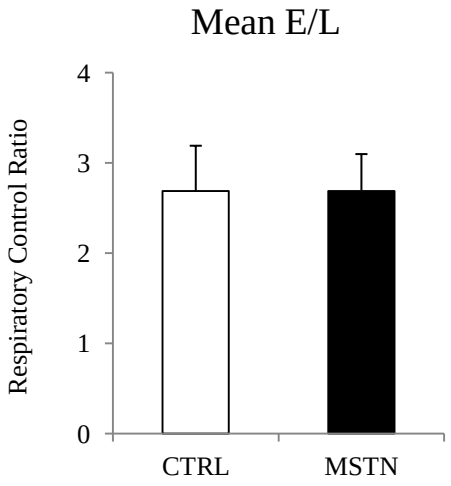

Figure 4-15: Respiratory control ratio in myotubes.

Ratio of the mass-specific oxygen flux of Electron Transport System; ETS (E) normalized to Leak (L) in six-day differentiated C2C12 myotubes in CTRL and MSTN groups. All values represent the mean ± SEM for CTRL (white bars, n=8) and MSTN (black bars, n=6) myotubes.

4.3.4 Liver

4.3.4.1 Mitochondrial Respiratory Capacity

Mass-specific oxygen fluxes; R, L or E showed no significant difference (p>0.05) between CTRL and MSTN groups, thus suggesting a preserved mitochondrial function upon MSTN treatment. All values represent the mean ± SEM for CTRL (white bars, n=3) and MSTN (black bars, n=3) liver cells.

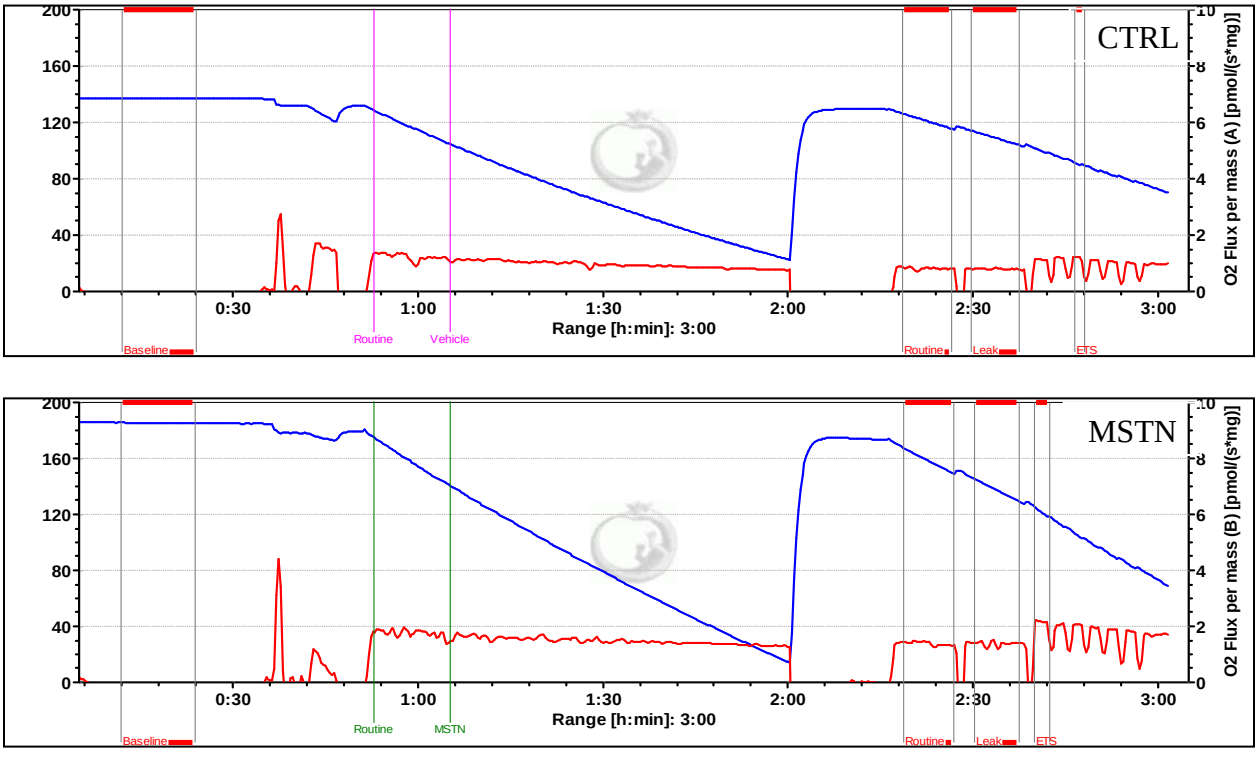

Figure 4-16: Oxygen flux per volume (pmol/s.ml) and oxygen concentration (µM) as a function of time in liver cells.

Representative charts showing oxygen flux per volume (pmol/s.ml) [red lines] and oxygen concentration (μM) [blue lines] corrected for instrumental background as a function of time in untreated (CTRL; top graph) and MSTN-treated (MSTN; bottom graph) liver cells. Marked sections are used to calculate the oxygen flux for ROUTINE and LEAK respiratory states. Baseline represents oxygen flux in the two chambers at full oxygen concentration.

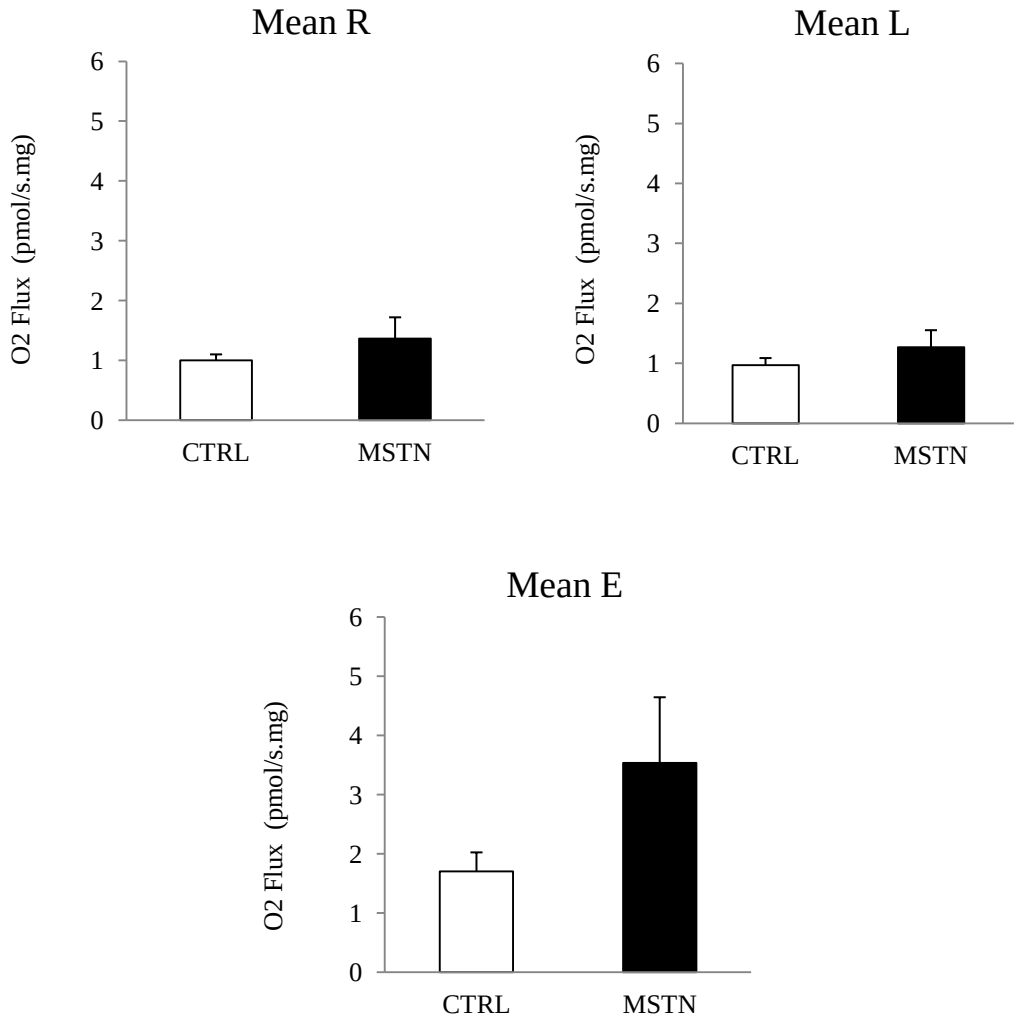

Figure 4-17: Mitochondrial respiratory capacity in liver cells.

Mass-specific oxygen fluxes of Routine (R), Leak (L) and Electron Transport System; ETS (E) respiration were assessed in 90% confluent murine liver cells in the absence and presence of MSTN (1.5ug/ml, 1 hour); CTRL and MSTN respectively. All values represent the mean ± SEM for CTRL (white bars, n=3) and MSTN (black bars, n=3) liver cells.

4.3.4.2 Coupling Control Ratios

Flux control ratios of mass-specific oxygen fluxes; (R/E) or (L/E) showed no significant difference (p>0.05) between CTRL and MSTN, thus suggesting no change in the coupling tightness of mitochondrial respiration upon MSTN treatment. All values represent the mean ± SEM for CTRL (white bars, n=3) and MSTN (black bars, n=3) liver cells.

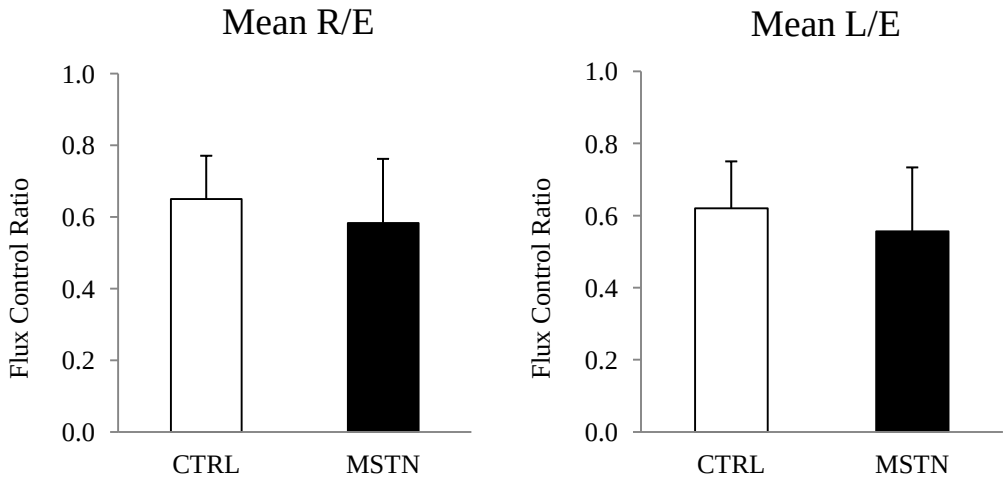

Figure 4-18: Coupling control ratios in liver cells.

Flux control ratios of mass-specific oxygen fluxes for Routine(R) and Leak (L) normalized to Electron Transport System; ETS (E) in 90% confluent murine liver cells in CTRL and MSTN groups. All values represent the mean ± SEM for CTRL (white bars, n=3) and MSTN (black bars, n=3) liver cells.

4.3.4.3 Respiratory Control Ratio

Respiratory control ratio; (E/L) showed no significant difference (p>0.05) between CTRL and MSTN groups, suggesting no change in mitochondrial integrity upon MSTN treatment. All values represent the mean ± SEM for CTRL (white bars, n=3) and MSTN (black bars, n=3) liver cells.

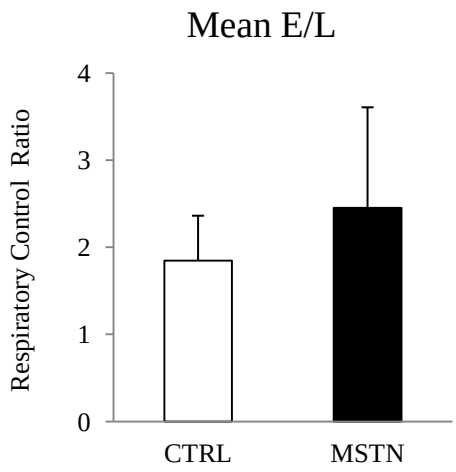

Figure 4-19: Respiratory control ratio in liver cells.

Ratio of the mass-specific oxygen flux of Electron Transport System; ETS (E) normalized to Leak (L) in 90% confluent murine liver cells in CTRL and MSTN group.

All values represent the mean ± SEM for CTRL (white bars, n=3) and MSTN (black bars, n=3) liver cells.

Chapter Five: **DISCUSSION**

5.1 Introduction

The purpose of this study was to further investigate the role of MSTN as a novel regulator of insulin resistance and carbohydrate metabolism in skeletal muscle and liver. There were three specific aims for this study (a) to investigate the role of MSTN in glucose metabolism and insulin sensitivity *in vivo* and *in vitro,* (b) to assess the role of AMPK involved in MSTN-regulated glucose metabolism *in vivo* and *in vitro,* and (c) to evaluate the effect of MSTN on glucose-dependent mitochondrial respiration *in vitro.*

5.2 Body Weight and Muscle Weight

The dose and duration of the recombinant MSTN treatment used in our study did not induce any significant changes in the weights of the bodies or the gastrocnemius muscle of the MSTN-treated mice compared to CTRL mice. This supports the notion that any potential MSTN-induced effects we observe will be independent of the changes in whole-body and/or muscle mass.

5.3 Role of myostatin in insulin sensitivity and glucose metabolism *in vivo* and *in vitro*

5.3.1 Myostatin effect on insulin sensitivity and glucose metabolism

Skeletal muscle and liver play a central role in preserving whole-body metabolic homeostasis not only as a result of being the most insulin-sensitive organs, but also because both of them comprise almost 45% of the total energy expenditure of the human body. Nonetheless, the cross-talk between their regulatory metabolic roles has not been fully elucidated yet. MSTN is a myokine reported to play a principal role in maintaining whole-body metabolic homeostasis (Lin, Arnold et al. 2002, McPherron and Lee 2002, Zimmers, Davies et al. 2002), therefore suggesting a potential role in this cross-talk.

Since glucose is one of the principal oxidative substrates whose metabolism disruption would result in IR, therefore we investigated the effect of MSTN on glucose metabolism and IS using various *in vivo* and *in vitro* methods. GTT done in mice revealed no significant differences in BGL over the 120-minutes period or after calculating AUC between the CTRL and MSTN groups. However, there was a trend towards a decreased AUC in MSTN-treated mice, suggesting an increased glucose uptake. Interestingly, this trend, although statistically non-significant, comes in accordance with previous unpublished observations from our lab, where GTT showed a significant increase in glucose uptake upon MSTN-treatment.

On the other hand, ITT showed that BGL at the time point “15 minutes” was significantly higher (p=0.043) in MSTN-treated group compared to CTRL group, although AUC showed no significant difference between the two groups (p=0.25).

Interestingly, the magnitude of MSTN-induced changes in ITT was similar to, but less than, that previously reported by Hittel *et al* (Hittel, Axelson et al. 2010), who described an induction of IR upon short-term administration of recombinant MSTN in mice.

Basal and insulin-stimulated glucose uptakes (2-DG) were determined *in vitro* in C2C12 and liver cells in the absence and presence of recombinant MSTN; CTRL and MSTN respectively. In C2C12 cells, one-hour treatment with recombinant MSTN showed no significant change compared to CTRL group; neither in basal nor in insulin-stimulated glucose uptake. However, in liver cells, one-hour treatment with recombinant MSTN significantly (p=0.047) reduced insulin-stimulated glucose uptake compared to CTRL group. Also, liver cells showed significantly (p=0.046) higher insulin-stimulated glucose uptake compared to basal glucose uptake in CTRL group but not in MSTN group. Taken together, these results suggest a decrease in insulin-stimulated glucose uptake upon short-term MSTN treatment.

The previous results from GTT and ITT, although paradoxical, suggest that the observed increase in glucose uptake seen in GTT potentially occurs via an insulin-independent mechanism. This notion was supported by the observations obtained from 2-DG assays, where the hepatic insulin-stimulated glucose uptake was significantly reduced after one-hour treatment with recombinant MSTN compared to CTRL group. Our observations from ITT and 2-DG, suggest that MSTN likely plays a role in interfering with insulin-stimulated glucose uptake, a role that comes in agreement with previous studies reporting MSTN-induced insulin resistance.

Our qRT-PCR results showed that MSTN treatment did not affect the glucose uptake in skeletal muscle, where *GLUT1* and *GLUT4* expression was not significantly increased

in gastrocnemius muscle from MSTN-treated mice compared to CTRL mice (c.f. Chen *et al.*). Contrarily, there was a tendency towards a significant (p= 0.053) reduction in the glucose transport gene; *GLUT1* in gastrocnemius muscle from MSTN-treated mice. In line with these results, 2-DG assays revealed that C2C12 did not show any significant increase in either basal or insulin-stimulated glucose uptake upon MSTN treatment. Therefore, our results do not support the notion of a MSTN-mediated increase in glucose uptake.

5.3.2 Myostatin effect on blood lactate and tissue glycogen

Our results showed that blood lactate, the product of cellular glycolysis, was not significantly changed by MSTN treatment compared to CTRL group, thus suggesting no change in cellular anaerobic glycolysis.

Interestingly, MSTN treatment showed a significant (p= 0.03) reduction in hepatic glycogen content compared to CTRL group, whereas it showed no significant change in muscle glycogen content (p= 0.22). Moreover, our qRT-PCR results showed a tendency towards a significant (p= 0.056) reduction in the expression of *GYG1* gene encoding for glycogenin in the gastrocnemius muscle from MSTN-treated mice compared to CTRL mice.

Previous reports showed that IR and T2D are associated with reduced glycogen content in skeletal muscle (Shulman, Rothman et al. 1990) and liver (Magnusson, Rothman et al. 1992). Therefore, based on previous reports and our current observations, we hypothesize that MSTN induces IR in mice, by impairing the sensitivity of skeletal

muscle and liver to insulin, resulting in a subsequent reduction in insulin-dependent glucose uptake. Glycogenesis, being a major pathway for glucose disposal, will consequently decrease due to the reduced availability of its principal substrate; glucose. This reduction in glycogen synthesis could accordingly result in decreased glycogenin production, since glycogenin is the self-glycosylating primer initiating glycogen granule formation.

In contrast to our current findings, Chen *et al* (Chen, Ye et al. 2010) reported that the MSTN-induced reduction in glycogen content was attributed to increased glycolysis. They also reported increased *GYG1* expression, which is seemingly inconsistent with their report of reduced glycogen content.

5.3.3 Myostatin effect on IL-6

IL-6, one of most well characterized myokines, was reported to increase insulin-stimulated glucose disposal in humans as well as increasing insulin-stimulated glucose uptake in vitro via an AMPK-dependent mechanism (Carey, Steinberg et al. 2006). Our results, revealed no significant increase in *IL-6* gene expression with MSTN treatment in mice compared to CTRL group.

5.3.4 Analysis of current study vs. previous reports

Our *in vitro* results are in accordance with our *in vivo* findings, suggesting that the main effect of exogenous recombinant MSTN on glucose metabolism and IS appears to be on liver, thus meriting further investigation of this metabolically critical organ.

In contrast to the findings of this study, Chen *et al* reported that they provided the -first- experimental evidence to show that recombinant MSTN directly regulated glucose metabolism in an AMPK-dependent manner, via promoting glycolysis and glucose uptake, as well as decreasing glycogen content in C2C12 myotubes; observations none of which we could reproduce in similarly conducted experiments.

In vitro observations reported by Chen *et al*, i.e. MSTN-induced increase in glucose consumption and glucose uptake in C2C12 myotubes, were in line with a previous report where MSTN overexpression in mice was shown to reduce BGL (Zimmers, Davies et al. 2002). However, the results reported by Chen *et al* were not questionable due to the lack of previous studies investigating the direct effect of MSTN on glucose metabolism. Nonetheless, there was solid evidence that lack of MSTN (e.g. MSTN-null mice) showed significantly enhanced glucose metabolism (McPherron and Lee 2002, Zhang, McFarlane et al. 2011). This suggests a dubious role for MSTN in regulating glucose metabolism *in vivo*.

5.4 Role of AMPK in myostatin-regulated glucose metabolism *in vivo* and *in vitro*

Several Smad-independent pathways were shown to play a role in the growth inhibition effects of MSTN, beside its canonical Smad-dependent signaling pathways (Zhu, Topouzis et al. 2004, Philip, Lu et al. 2005, Huang, Chen et al. 2007, Yang, Zhang et al. 2007).

Being a metabolic master switch, AMPK plays a key role in orchestrating multiple metabolic processes including; cellular glucose uptake, GLUT4 biogenesis, the β-oxidation of fatty acids and mitochondrial biogenesis (Winder 2001). AMPK activity is determined by energy status of the cell, particularly intracellular AMP/ATP ratio and glycogen content (McBride, Ghilagaber et al. 2009).

We carried out western blots to determine the protein expression levels of phosphorylated and total AMPKα as well as its target protein; ACC in skeletal muscle and liver. Normalized densitometric analysis for the phosphorylated AMPKα (Thr172) and ACC (Ser79) protein levels in gastrocnemius muscle and liver revealed that neither pAMPK nor pACC showed any significant difference (p>0.05) in their protein expression with MSTN treatment when compared to CTRL group. Similar findings were observed when performing similar western blots in vehicle-treated (CTRL) and MSTN-treated (MSTN) C2C12 myotubes as well as liver cells. Our findings rule out the likelihood that exogenous recombinant MSTN possess any direct effect on the AMPK metabolic regulatory pathway.

Contrarily, Chen *et al.* (Chen, Ye et al. 2010) reported that the AMPK signalling pathway was activated in MSTN-treated C2C12 myotubes, where recombinant MSTN

could decrease cellular ATP concentration and glycogen levels in C2C12 myotubes, thus activating AMPK. Paradoxically, Zhang *et al* reported a significant increase in the levels and activity of AMPK, in *Mstn* $^{-/-}$ mice, causing the phosphorylation and subsequent inhibition of the downstream target enzyme; ACC. This results in decreased expression of malonyl-CoA, which - in turn - limits de novo synthesis of fatty acids with a concurrent increase in beta-oxidation of fatty acids. This observation was in accordance with both the decreased fat mass and reduced IR seen in these *Mstn* $^{-/-}$ mice, thus they proposed a mechanism whereby MSTN negatively regulated the levels of AMPK in peripheral tissues, therefore influencing IS. In addition to reduced adiposity, MSTN absence or inhibition enhanced glucose tolerance and IS, via increased insulin signalling, as confirmed by increased GLUT4 levels and increased Akt phosphorylation (Zhang, McFarlane et al. 2011).

Zhang *et al* hypothesized that improved IS in *Mstn* $^{-/-}$ mice is due to enhanced AMPK levels. This hypothesis was supported by earlier reports that acute AMPK activation (3.5 hours) improved insulin-mediated glucose uptake via increasing GLUT4 levels (Fisher, Gao et al. 2002), and that chronic AMPK activation (8 weeks) improved whole-body IS in insulin-resistant Zucker rats (Pold, Jensen et al. 2005). In addition, it was reported that muscle-specific AMPK ablation in transgenic mice resulted in fully blunted insulin-stimulated glucose transport and exacerbated IR by high-fat feeding (Fujii, Ho et al. 2008).

Zhang *et al* (Zhang, McFarlane et al. 2011) attributed the contradiction between their own results and those reported by Chen *et al.* (Chen, Ye et al. 2010) to the differences between the two experimental models used. Suggesting that treatment with recombinant

MSTN protein (Chen, Ye et al. 2010) could have caused a negative energy balance via MSTN-induced cachexia in C2C12 myotubes (Fisher, Gao et al. 2002, Zimmers, Davies et al. 2002), resulting in an increased AMP/ATP ratio which would eventually trigger AMPK activation. We also suggest that MSTN-associated activation of AMPK could happen due to LPS contamination of recombinant MSTN. Especially that LPS was described to show an increased activation of the IGF-1/Akt/mTOR pathway in L6 myotubes, in a way similar to that seen in cachexic conditions, as well as a TNF-alpha-dependent increase of MSTN level, where the latter lacks bioactivity; i.e. inducing no change in ubiquitin-proteasome pathway or myogenic differentiation capacity (Bradley M Elliot, MSc Thesis, 2009).

We were also concerned that our source of recombinant MSTN (R&D Systems) may not be free of LPS contamination. Not to mention that we, as well as other colleagues from a different laboratory, experienced significant lot-to-lot variations with the recombinant MSTN supplied by R&D Systems. Consequently, we switched our source of recombinant MTSN to PeproTech (Rocky Hill, USA) for our *in vitro* experiments.

Given the inability to confirm the results of Chen *et al.*, we sought to validate our recombinant MSTN by monitoring the phosphorylation of Smad2. We were capable of demonstrating that the level of phosphorylated Smad2 (S465/467) proteins were increased in C2C12 myoblasts, in six-day differentiated C2C12 myotubes and in liver cells when treated with recombinant MSTN (MSTN) in comparison to untreated cells (CTRL). These findings provide experimental evidence for the activation of the transcription factors Smad2/3 in response to recombinant MSTN, thus inducing MSTN-specific gene regulation which results in the inhibition of differentiation of C2C12

myoblasts into mature myotubes. However, as mentioned earlier, our Western blotting did not show any significant change in the phosphorylation levels of AMPK or ACC protein with MSTN-treatment.

5.5 Myostatin effect on glucose-dependent in situ mitochondrial respiration

Since AMPK is a major metabolic switch that orchestrates the switch between glycolysis/ fatty acid metabolism and mitochondrial oxidative metabolism, we aimed in this study to investigate whether MSTN would possibly have any AMPK-mediated effect on mitochondrial respiration. Therefore, we adopted an *in vitro* model of MSTN-induced atrophy in C2C12 myotubes to investigate the reported MSTN-induced changes in glucose metabolism and IS; particularly to determine the effect of MSTN on glucose-dependent mitochondrial respiration. This study would be the first – to date – to investigate glucose-dependent mitochondrial respiration in C2C12 myotubes and 1C1C7 liver cells in response to recombinant MSTN treatment *in vitro.*

Cellular respirometry measures respiration in mitochondria, either isolated or in permeabilized tissues and cells. Cellular or mitochondrial respirometry has the property of measuring the rate of oxygen consumption by the mitochondria, thus being the principal tool for studying mitochondrial function, without involving an entire living animal. Isolated mitochondria as well as permeabilized tissue or cells are usually the candidate samples for measuring mitochondrial respiration.

We assessed mitochondrial function in C2C12 myotubes and in liver cells via high-resolution respirometry (HRR) using OROBOROS Oxygraph-2k (O2k). We applied the

phosphorylation control protocol (PCP) to assess: (1) Cellular ROUTINE respiration (State R); which is the aerobic metabolic activity under routine culture conditions, (2) Oligomycin-inhibited LEAK respiration (State L, State 4), which is due to the compensation for the proton leak in response to ATP synthase inhibition (Complex V) and (3) FCCP-stimulated respiration, which is the electron transfer system (ETS) capacity at non-coupled respiration of intact cells (State E, State 3u).

We made use of PCP to obtain information about the flux control ratios (FCRs); ROUTINE and LEAK flux control ratios. The ROUTINE flux control ratio (R/E) is a measurement of how close ROUTINE respiration operates compared to the respiratory capacity of the ETS, while the LEAK flux control ratio (L/E) is a measurement of the degree of uncoupling at a constant ETS capacity. The magnitude of L/E increases as uncoupling increases; from a theoretical minimum of "0" for a fully coupled system to a maximum of "1" for a fully uncoupled/non-coupled system. In intact cells, FCRs are also referred to as coupling control ratios (CCRs).

Our HRR data showed no significant changes (p>0.05) in R, L or E with MSTN treatment compared to CTRL group, neither in C2C12 myotubes, nor in liver cells. Also, upon calculating CCRs, there was no significant difference (p>0.05) in ratios of (R/E) or (L/E) between CTRL and MSTN groups. Therefore, our results show that recombinant MSTN treatment could not induce any changes in glucose-dependent mitochondrial respiration; where C2C12 myotubes and liver cells could preserve their aerobic metabolic capacity without any significant uncoupling.

These findings, consistent with the results of our previously mentioned experiments, show that there was not any noticeable glycolytic shift in the mitochondrial respiration

upon recombinant MSTN treatment of C2C12 myotubes or liver cells. Thus, our HRR data come to further confirm our observations that recombinant MSTN likely plays no direct role in promoting glycolysis in myotubes or liver cells.

Previous reports show that chemical activation of AMPK, with AICAR in rat muscle, increased the mitochondrial enzymes and increased GLUT4 and hexokinase activity. Therefore it was proposed that the activation of AMPK accompanying muscle contraction during training have a potential effect on the biochemical adaptations to chronic energy stress (Winder, Holmes et al. 2000). Also, AMPK was shown to stimulate mitochondrial biogenesis and expression of respiratory proteins (Bergeron, Ren et al. 2001).

There were reports that the loss of MSTN expression is accompanied with a concomitant reduction in mitochondrial content, that results in impaired muscle oxidative capacity compared to WT mice (Amthor, Macharia et al. 2007, Lipina, Kendall et al. 2010, Savage and McPherron 2010). Also, it was reported that electro-stimulated exercise in MSTN-deficient mice, revealed a reduced oxidative mitochondrial capacity compared to WT mice (Baligand, Gilson et al. 2010).

Recently, Ploquin *et al* reported they have investigated - for the first time – the mitochondrial content and function according to their subcellular location in MSTN-null skeletal muscle. Their results showed that MSTN deficiency resulted in an increased skeletal muscle mass, as well as uncoupling of the respiration of intermyofibrillar mitochondria of glycolytic muscles, resulting in a reduction in the muscular response to endurance exercise (Ploquin, Chabi et al. 2012).

Based on observations from previously mentioned reports that describe a reduction in mitochondrial count and/or function associated with MSTN deficiency, we expected to find an antithetical result to our current data; i.e. a theoretically positive correlation between mitochondrial function and recombinant MSTN treatment. However, we noticed no difference between CTRL and MSTN groups.

A possible explanation would be the fundamentally different experimental model. All those studies were conducted in MSTN-null mice, where MSTN has been constitutively inhibited in a prenatal stage. Therefore, it would be questionable whether the mitochondrial effects observed in the MSTN-null animals are exclusively due to the lack of MSTN protein itself. Moreover, the reduced mitochondrial function was usually due to decreased biogenesis which was explained to be partially a result of the lower relative proportion of oxidative fibers in MSTN-deficient skeletal muscle (Girgenrath, Song et al. 2005, Steelman, Recknor et al. 2006). It is worth mentioning that the use of MSTN antagonists (e.g. anti-MSTN antibodies) in adult mice or the attempts for post-developmental MSTN knockout did not reveal any changes in the mitochondrial content (Girgenrath, Song et al. 2005) or the expression of mitochondrial proteins (Welle, Cardillo et al. 2009).

Numerous studies conducted in MSTN-null animals - with prenatal constitutive inhibition of the *Mstn* gene - suggest that MSTN antagonists would be useful in improving IS during obesity and could present a pharmacological tool to treat/prevent obesity as well as muscle degenerative disorders. In humans, however, the treatment of such diseases usually takes place in the skeletal muscle of adults. Therefore, further studies with post-developmental inhibition of MSTN function, including mitochondrial

metabolism, are inevitably necessary to investigate the feasibility of using MSTN antagonists as a therapeutic tool for various disorders of skeletal muscle metabolism as well as obesity control and treatment.

5.6 Summary

The primary findings of this study have shown **(i)** a tendency towards decreased glucose uptake (*in vivo*; ITT), supported by the MSTN-induced significant reduction in insulin-stimulated hepatic glucose uptake compared to basal glucose uptake (*in vitro;* 2-DG), **(ii)** a significant reduction in hepatic glycogen content (*in vivo*), which is in line with a tendency towards significant reduction in muscle-expressed *GYG1* (*in vivo*), both in accordance with previously reported reduction in hepatic and muscular glycogen content associated with IR, **(iii)** the lack of significant change in phosphorylated or total protein levels of AMPK or ACC with MSTN-treatment neither *in vivo* nor *in vitro,* and finally **(iv)** the lack of significant change in mitochondrial respiratory capacity in MSTN-treated group.

Taken together, our *in vivo* and *in vitro* findings suggest that exogenous MSTN plays an important role in reducing hepatic IS, thus reducing hepatic glucose uptake and glycogen content with the preservation of the mitochondrial respiratory capacity of skeletal muscle and liver.

5.7 Strengths

5.7.1 Novelty

This study is amongst the first studies that investigates the direct effect of exogenous MSTN on glucose metabolism and IS both *in vivo* and *in vitro*. Also, this is the first study –to date- to investigate the direct effect of exogenous MSTN on glucose metabolism at a mitochondrial level using high-resolution respirometry.

This study provides evidence supporting the role of MSTN in inducing IR *in vivo*, as well as suggesting a potential role of liver in the MSTN-induced IR, thus presenting liver as a worthy future target of investigation to elucidate the development of IR.

5.7.2 Exogenous Myostatin

The use of exogenous MSTN in adult WT mice would provide information about the direct effect of MSTN on the metabolic processes, precisely glucose metabolism and IS. Administration of exogenous MSTN would have the advantage of offering a more accurate simulation of the pathological conditions involving increased MSTN levels in humans, rather than the conditions created by constitutive MSTN inhibition in null animals. Moreover, investigating the direct effects of MSTN avoids potential undetected metabolic changes or altered feedback mechanisms resulting from the constitutive MSTN inhibition in null animals.

5.8 Limitations / Areas of Improvement

5.8.1 Myostatin Source

The obligation to use a different source of recombinant MSTN for *in vitro* experiments other than that used for the *in vivo* work was one of the limitations of this study. However, the lack of reproducibility in results upon using recombinant MSTN from R&D Systems necessitated a change of the provider.

5.8.2 Lactate and Glycogen Measurement

A possible limitation can be the lack of the assessment of the activity of glycogen synthase and glycogen phosphorylase enzymes. Assessing enzyme activities would provide a more comprehensive understanding of the state of glycogenesis and glycogenolysis upon exogenous MSTN treatment. Also using primers for GYG2 for the qRT-PCR assessment of glycogenin in liver would provide more accurate results as it is predominantly expressed in liver.

A potential area of improvement would have been using portable lactate meters during GTT and ITT to detect acute changes in blood lactate levels in mice upon exogenous MSTN administration.

5.8.3 High-Resolution Respirometry

A limitation in the assessment of mitochondrial respiratory capacity in liver cells was the lower number of sample; n=3, rather than six.

5.9 Conclusion and Future Directions

Altogether, this study sheds some light on the potential role of liver in MSTN-induced IR, which necessitates further investigation of the role of MSTN in this promising and metabolically critical organ. We intend to investigate and quantify IR in liver as well as skeletal muscle using hyperinsulinemic-euglycemic clamps, and radioactive tracers such as [3-^{3}H] glucose to assess real-time glucose uptake in tissues *in vivo*.

The elucidation of the metabolic functions of MSTN will help us understand the role of skeletal muscle and liver in regulating whole-body metabolic homeostasis and will offer opportunities to develop novel therapeutic approaches for the treatment of IR involved in T2D and various metabolic syndromes.

References

Akpan, I., M. D. Goncalves, R. Dhir, X. Yin, E. E. Pistilli, S. Bogdanovich, T. S. Khurana, J. Ucran, J. Lachey and R. S. Ahima (2009). "The effects of a soluble activin type IIB receptor on obesity and insulin sensitivity." International journal of obesity **33**(11): 1265-1273.

Allen, D. L., A. S. Cleary, K. J. Speaker, S. F. Lindsay, J. Uyenishi, J. M. Reed, M. C. Madden and R. S. Mehan (2008). "Myostatin, activin receptor IIb, and follistatin-like-3 gene expression are altered in adipose tissue and skeletal muscle of obese mice." American journal of physiology. Endocrinology and metabolism **294**(5): E918-927.

Amthor, H., R. Macharia, R. Navarrete, M. Schuelke, S. C. Brown, A. Otto, T. Voit, F. Muntoni, G. Vrbova, T. Partridge, P. Zammit, L. Bunger and K. Patel (2007). "Lack of myostatin results in excessive muscle growth but impaired force generation." Proceedings of the National Academy of Sciences of the United States of America **104**(6): 1835-1840.

Anderson, S. B., A. L. Goldberg and M. Whitman (2008). "Identification of a novel pool of extracellular pro-myostatin in skeletal muscle." The Journal of biological chemistry **283**(11): 7027-7035.

Antony, N., J. J. Bass, C. D. McMahon and M. D. Mitchell (2007). "Myostatin regulates glucose uptake in BeWo cells." American journal of physiology. Endocrinology and metabolism **293**(5): E1296-1302.

Baligand, C., H. Gilson, J. C. Menard, O. Schakman, C. Wary, J. P. Thissen and P. G. Carlier (2010). "Functional assessment of skeletal muscle in intact mice lacking myostatin by concurrent NMR imaging and spectroscopy." Gene Ther **17**(3): 328-337.

Bartoli, M., J. Poupiot, A. Vulin, F. Fougerousse, L. Arandel, N. Daniele, C. Roudaut, F. Noulet, L. Garcia, O. Danos and I. Richard (2007). "AAV-mediated delivery of a mutated myostatin propeptide ameliorates calpain 3 but not alpha-sarcoglycan deficiency." Gene therapy **14**(9): 733-740.

Bellinge, R. H., D. A. Liberles, S. P. Iaschi, A. O'Brien P and G. K. Tay (2005). "Myostatin and its implications on animal breeding: a review." Animal genetics **36**(1): 1-6.

Benny Klimek, M. E., T. Aydogdu, M. J. Link, M. Pons, L. G. Koniaris and T. A. Zimmers (2010). "Acute inhibition of myostatin-family proteins preserves skeletal muscle in mouse models of cancer cachexia." Biochemical and biophysical research communications **391**(3): 1548-1554.

Bergeron, R., J. M. Ren, K. S. Cadman, I. K. Moore, P. Perret, M. Pypaert, L. H. Young, C. F. Semenkovich and G. I. Shulman (2001). "Chronic activation of AMP kinase results in NRF-1 activation and mitochondrial biogenesis." Am J Physiol Endocrinol Metab **281**(6): E1340-1346.

Bergeron, R., R. R. Russell, 3rd, L. H. Young, J. M. Ren, M. Marcucci, A. Lee and G. I. Shulman (1999). "Effect of AMPK activation on muscle glucose metabolism in conscious rats." Am J Physiol **276**(5 Pt 1): E938-944.

Bernardo, B. L., T. S. Wachtmann, P. G. Cosgrove, M. Kuhn, A. C. Opsahl, K. M. Judkins, T. B. Freeman, J. R. Hadcock and N. K. LeBrasseur (2010). "Postnatal PPARdelta activation and myostatin inhibition exert distinct yet complimentary effects on the metabolic profile of obese insulin-resistant mice." PloS one **5**(6): e11307.

Carey, A. L., G. R. Steinberg, S. L. Macaulay, W. G. Thomas, A. G. Holmes, G. Ramm, O. Prelovsek, C. Hohnen-Behrens, M. J. Watt, D. E. James, B. E. Kemp, B. K. Pedersen and M. A. Febbraio (2006). "Interleukin-6 increases insulin-stimulated glucose disposal in humans and glucose uptake and fatty acid oxidation in vitro via AMP-activated protein kinase." Diabetes **55**(10): 2688-2697.

Carling, D. and D. G. Hardie (1989). "The substrate and sequence specificity of the AMP-activated protein kinase. Phosphorylation of glycogen synthase and phosphorylase kinase." Biochim Biophys Acta **1012**(1): 81-86.

Carnac, G., S. Ricaud, B. Vernus and A. Bonnieu (2006). "Myostatin: biology and clinical relevance." Mini reviews in medicinal chemistry **6**(7): 765-770.

Catipovic, B. (2004). "Myostatin mutation associated with gross muscle hypertrophy in a child." The New England journal of medicine **351**(10): 1030-1031; author reply 1030-1031.

CDA (2009). An economic tsunami, the cost of diabetes in Canada. Toronto, ON, Canada, Canadian Diabetes Association.

Chen, Y., J. Ye, L. Cao, Y. Zhang, W. Xia and D. Zhu (2010). "Myostatin regulates glucose metabolism via the AMP-activated protein kinase pathway in skeletal muscle cells." Int J Biochem Cell Biol **42**(12): 2072-2081.

Clop, A., F. Marcq, H. Takeda, D. Pirottin, X. Tordoir, B. Bibe, J. Bouix, F. Caiment, J. M. Elsen, F. Eychenne, C. Larzul, E. Laville, F. Meish, D. Milenkovic, J. Tobin, C. Charlier and M. Georges (2006). "A mutation creating a potential illegitimate microRNA target site in the myostatin gene affects muscularity in sheep." Nature genetics **38**(7): 813-818.

Corton, J. M., J. G. Gillespie and D. G. Hardie (1994). "Role of the AMP-activated protein kinase in the cellular stress response." Curr Biol **4**(4): 315-324.

Davies, S. P., N. R. Helps, P. T. Cohen and D. G. Hardie (1995). "5'-AMP inhibits dephosphorylation, as well as promoting phosphorylation, of the AMP-activated protein kinase. Studies using bacterially expressed human protein phosphatase-2C alpha and native bovine protein phosphatase-2AC." FEBS Lett **377**(3): 421-425.

DeFronzo, R. A., J. D. Tobin and R. Andres (1979). "Glucose clamp technique: a method for quantifying insulin secretion and resistance." The American journal of physiology **237**(3): E214-223.

DeFronzo, R. A. and D. Tripathy (2009). "Skeletal muscle insulin resistance is the primary defect in type 2 diabetes." Diabetes care **32 Suppl 2**: S157-163.

Durante, P. E., K. J. Mustard, S. H. Park, W. W. Winder and D. G. Hardie (2002). "Effects of endurance training on activity and expression of AMP-activated protein kinase isoforms in rat muscles." Am J Physiol Endocrinol Metab **283**(1): E178-186.

Febbraio, M. A. and B. K. Pedersen (2005). "Contraction-induced myokine production and release: is skeletal muscle an endocrine organ?" Exerc Sport Sci Rev **33**(3): 114-119.

Feldman, B. J., R. S. Streeper, R. V. Farese, Jr. and K. R. Yamamoto (2006). "Myostatin modulates adipogenesis to generate adipocytes with favorable metabolic effects." Proceedings of the National Academy of Sciences of the United States of America **103**(42): 15675-15680.

Fisher, J. S., J. Gao, D. H. Han, J. O. Holloszy and L. A. Nolte (2002). "Activation of AMP kinase enhances sensitivity of muscle glucose transport to insulin." Am J Physiol Endocrinol Metab **282**(1): E18-23.

Flanagan, J. N., K. Linder, N. Mejhert, E. Dungner, K. Wahlen, P. Decaunes, M. Ryden, P. Bjorklund, S. Arver, S. Bhasin, A. Bouloumie, P. Arner and I. Dahlman (2009). "Role of follistatin in promoting adipogenesis in women." The Journal of clinical endocrinology and metabolism **94**(8): 3003-3009.

Foster, K., I. R. Graham, A. Otto, H. Foster, C. Trollet, P. J. Yaworsky, F. S. Walsh, D. Bickham, N. A. Curtin, S. L. Kawar, K. Patel and G. Dickson (2009). "Adeno-associated virus-8-mediated intravenous transfer of myostatin propeptide leads to systemic functional improvements of slow but not fast muscle." Rejuvenation research **12**(2): 85-94.

Fujii, N., R. C. Ho, Y. Manabe, N. Jessen, T. Toyoda, W. L. Holland, S. A. Summers, M. F. Hirshman and L. J. Goodyear (2008). "Ablation of AMP-activated protein kinase alpha2 activity exacerbates insulin resistance induced by high-fat feeding of mice." Diabetes **57**(11): 2958-2966.

Fujii, N., N. Jessen and L. J. Goodyear (2006). "AMP-activated protein kinase and the regulation of glucose transport." Am J Physiol Endocrinol Metab **291**(5): E867-877.

Gamer, L. W., N. M. Wolfman, A. J. Celeste, G. Hattersley, R. Hewick and V. Rosen (1999). "A novel BMP expressed in developing mouse limb, spinal cord, and tail bud is a potent mesoderm inducer in Xenopus embryos." Developmental biology **208**(1): 222-232.

Girgenrath, S., K. Song and L. A. Whittemore (2005). "Loss of myostatin expression alters fiber-type distribution and expression of myosin heavy chain isoforms in slow- and fast-type skeletal muscle." Muscle & nerve **31**(1): 34-40.

Grobet, L., D. Pirottin, F. Farnir, D. Poncelet, L. J. Royo, B. Brouwers, E. Christians, D. Desmecht, F. Coignoul, R. Kahn and M. Georges (2003). "Modulating skeletal muscle mass by postnatal, muscle-specific inactivation of the myostatin gene." Genesis **35**(4): 227-238.

Guo, T., W. Jou, T. Chanturiya, J. Portas, O. Gavrilova and A. C. McPherron (2009). "Myostatin inhibition in muscle, but not adipose tissue, decreases fat mass and improves insulin sensitivity." PloS one **4**(3): e4937.

Haidet, A. M., L. Rizo, C. Handy, P. Umapathi, A. Eagle, C. Shilling, D. Boue, P. T. Martin, Z. Sahenk, J. R. Mendell and B. K. Kaspar (2008). "Long-term enhancement of skeletal muscle mass and strength by single gene administration of myostatin inhibitors." Proceedings of the National Academy of Sciences of the United States of America **105**(11): 4318-4322.

Hawley, S. A., J. Boudeau, J. L. Reid, K. J. Mustard, L. Udd, T. P. Makela, D. R. Alessi and D. G. Hardie (2003). "Complexes between the LKB1 tumor suppressor, STRAD alpha/beta and MO25 alpha/beta are upstream kinases in the AMP-activated protein kinase cascade." J Biol **2**(4): 28.

Hayashi, T., M. F. Hirshman, N. Fujii, S. A. Habinowski, L. A. Witters and L. J. Goodyear (2000). "Metabolic stress and altered glucose transport: activation of AMP-activated protein kinase as a unifying coupling mechanism." Diabetes **49**(4): 527-531.

Hayashi, T., M. F. Hirshman, E. J. Kurth, W. W. Winder and L. J. Goodyear (1998). "Evidence for 5' AMP-activated protein kinase mediation of the effect of muscle contraction on glucose transport." Diabetes **47**(8): 1369-1373.

Hill, J. J., M. V. Davies, A. A. Pearson, J. H. Wang, R. M. Hewick, N. M. Wolfman and Y. Qiu (2002). "The myostatin propeptide and the follistatin-related gene are inhibitory binding proteins of myostatin in normal serum." The Journal of biological chemistry **277**(43): 40735-40741.

Hill, J. J., Y. Qiu, R. M. Hewick and N. M. Wolfman (2003). "Regulation of myostatin in vivo by growth and differentiation factor-associated serum protein-1: a novel protein with protease inhibitor and follistatin domains." Molecular endocrinology **17**(6): 1144-1154.

Hirai, S., H. Matsumoto, N. Hino, H. Kawachi, T. Matsui and H. Yano (2007). "Myostatin inhibits differentiation of bovine preadipocyte." Domestic animal endocrinology **32**(1): 1-14.

Hirai, S., H. Matsumoto, N. H. Moriya, H. Kawachi and H. Yano (2007). "Follistatin rescues the inhibitory effect of activin A on the differentiation of bovine preadipocyte." Domestic animal endocrinology **33**(3): 269-280.

Hittel, D. S., M. Axelson, N. Sarna, J. Shearer, K. M. Huffman and W. E. Kraus (2010). "Myostatin decreases with aerobic exercise and associates with insulin resistance." Med Sci Sports Exerc **42**(11): 2023-2029.

Hittel, D. S., J. R. Berggren, J. Shearer, K. Boyle and J. A. Houmard (2009). "Increased secretion and expression of myostatin in skeletal muscle from extremely obese women." Diabetes **58**(1): 30-38.

Hocquette, J. F., P. Bas, D. Bauchart, M. Vermorel and Y. Geay (1999). "Fat partitioning and biochemical characteristics of fatty tissues in relation to plasma metabolites and hormones in normal and double-muscled young growing bulls." Comp Biochem Physiol A Mol Integr Physiol **122**(1): 127-138.

Huang, Z., D. Chen, K. Zhang, B. Yu, X. Chen and J. Meng (2007). "Regulation of myostatin signaling by c-Jun N-terminal kinase in C2C12 cells." Cell Signal **19**(11): 2286-2295.

Hundal, H. S., P. J. Bilan, T. Tsakiridis, A. Marette and A. Klip (1994). "Structural disruption of the trans-Golgi network does not interfere with the acute stimulation of glucose and amino acid uptake by insulin-like growth factor I in muscle cells." Biochem J **297 (Pt 2)**: 289-295.

IDF (2011). Diabetes Atlas, Impaired Glucose Intolerance, International Diabetes Federation.

IDF (2011). IDF Diabetes Atlas. Brussels, Belgium, International Diabetes Federation.

Iglesias, M. A., J. M. Ye, G. Frangioudakis, A. K. Saha, E. Tomas, N. B. Ruderman, G. J. Cooney and E. W. Kraegen (2002). "AICAR administration causes an apparent enhancement of muscle and liver insulin action in insulin-resistant high-fat-fed rats." Diabetes **51**(10): 2886-2894.

Izumiya, Y., T. Hopkins, C. Morris, K. Sato, L. Zeng, J. Viereck, J. A. Hamilton, N. Ouchi, N. K. LeBrasseur and K. Walsh (2008). "Fast/Glycolytic muscle fiber growth

reduces fat mass and improves metabolic parameters in obese mice." Cell metabolism **7**(2): 159-172.

Jessen, N., R. Pold, E. S. Buhl, L. S. Jensen, O. Schmitz and S. Lund (2003). "Effects of AICAR and exercise on insulin-stimulated glucose uptake, signaling, and GLUT-4 content in rat muscles." J Appl Physiol **94**(4): 1373-1379.

Ji, M., Q. Zhang, J. Ye, X. Wang, W. Yang and D. Zhu (2008). "Myostatin induces p300 degradation to silence cyclin D1 expression through the PI3K/PTEN/Akt pathway." Cellular signalling **20**(8): 1452-1458.

Joulia-Ekaza, D. and G. Cabello (2007). "The myostatin gene: physiology and pharmacological relevance." Current opinion in pharmacology **7**(3): 310-315.

Kristiansen, S. B., L. Solskov, N. Jessen, B. Lofgren, O. Schmitz, J. E. Nielsen-Kudsk, T. T. Nielsen, H. E. Botker and S. Lund (2009). "5-Aminoimidazole-4-carboxamide-1-beta-D-ribofuranoside increases myocardial glucose uptake during reperfusion and induces late pre-conditioning: potential role of AMP-activated protein kinase." Basic Clin Pharmacol Toxicol **105**(1): 10-16.

Kurth-Kraczek, E. J., M. F. Hirshman, L. J. Goodyear and W. W. Winder (1999). "5' AMP-activated protein kinase activation causes GLUT4 translocation in skeletal muscle." Diabetes **48**(8): 1667-1671.

Langley, B., M. Thomas, A. Bishop, M. Sharma, S. Gilmour and R. Kambadur (2002). "Myostatin inhibits myoblast differentiation by down-regulating MyoD expression." The Journal of biological chemistry **277**(51): 49831-49840.

Langley, B., M. Thomas, C. McFarlane, S. Gilmour, M. Sharma and R. Kambadur (2004). "Myostatin inhibits rhabdomyosarcoma cell proliferation through an Rb-independent pathway." Oncogene **23**(2): 524-534.

LeBrasseur, N. K., T. M. Schelhorn, B. L. Bernardo, P. G. Cosgrove, P. M. Loria and T. A. Brown (2009). "Myostatin inhibition enhances the effects of exercise on performance and metabolic outcomes in aged mice." The journals of gerontology. Series A, Biological sciences and medical sciences **64**(9): 940-948.

Lee, S. J. (2004). "Regulation of muscle mass by myostatin." Annual review of cell and developmental biology **20**: 61-86.

Lee, S. J. (2007). "Quadrupling muscle mass in mice by targeting TGF-beta signaling pathways." PloS one **2**(8): e789.

Lee, S. J. (2007). "Sprinting without myostatin: a genetic determinant of athletic prowess." Trends in genetics : TIG **23**(10): 475-477.

Lee, S. J., L. A. Reed, M. V. Davies, S. Girgenrath, M. E. Goad, K. N. Tomkinson, J. F. Wright, C. Barker, G. Ehrmantraut, J. Holmstrom, B. Trowell, B. Gertz, M. S. Jiang, S. M. Sebald, M. Matzuk, E. Li, L. F. Liang, E. Quattlebaum, R. L. Stotish and N. M. Wolfman (2005). "Regulation of muscle growth by multiple ligands signaling through activin type II receptors." Proceedings of the National Academy of Sciences of the United States of America **102**(50): 18117-18122.

Lee, S. W., G. Dai, Z. Hu, X. Wang, J. Du and W. E. Mitch (2004). "Regulation of muscle protein degradation: coordinated control of apoptotic and ubiquitin-proteasome systems by phosphatidylinositol 3 kinase." Journal of the American Society of Nephrology : JASN **15**(6): 1537-1545.

Leong, G. M., A. J. Kee, S. M. Millard, N. Martel, N. Eriksson, N. Turner, G. J. Cooney, E. C. Hardeman and G. E. Muscat (2010). "The Ski proto-oncogene regulates body composition and suppresses lipogenesis." International journal of obesity **34**(3): 524-536.

Lillioja, S., D. M. Mott, B. V. Howard, P. H. Bennett, H. Yki-Jarvinen, D. Freymond, B. L. Nyomba, F. Zurlo, B. Swinburn and C. Bogardus (1988). "Impaired glucose tolerance as a disorder of insulin action. Longitudinal and cross-sectional studies in Pima Indians." The New England journal of medicine **318**(19): 1217-1225.

Lin, J., H. B. Arnold, M. A. Della-Fera, M. J. Azain, D. L. Hartzell and C. A. Baile (2002). "Myostatin knockout in mice increases myogenesis and decreases adipogenesis." Biochem Biophys Res Commun **291**(3): 701-706.

Lipina, C., H. Kendall, A. C. McPherron, P. M. Taylor and H. S. Hundal (2010). "Mechanisms involved in the enhancement of mammalian target of rapamycin signalling and hypertrophy in skeletal muscle of myostatin-deficient mice." FEBS Lett **584**(11): 2403-2408.

Magnusson, I., D. L. Rothman, L. D. Katz, R. G. Shulman and G. I. Shulman (1992). "Increased rate of gluconeogenesis in type II diabetes mellitus. A 13C nuclear magnetic resonance study." J Clin Invest **90**(4): 1323-1327.

Martin, T. L., T. Alquier, K. Asakura, N. Furukawa, F. Preitner and B. B. Kahn (2006). "Diet-induced obesity alters AMP kinase activity in hypothalamus and skeletal muscle." J Biol Chem **281**(28): 18933-18941.

Matsakas, A., K. Foster, A. Otto, R. Macharia, M. I. Elashry, S. Feist, I. Graham, H. Foster, P. Yaworsky, F. Walsh, G. Dickson and K. Patel (2009). "Molecular, cellular and physiological investigation of myostatin propeptide-mediated muscle growth in adult mice." Neuromuscular disorders : NMD **19**(7): 489-499.

McBride, A., S. Ghilagaber, A. Nikolaev and D. G. Hardie (2009). "The glycogen-binding domain on the AMPK beta subunit allows the kinase to act as a glycogen sensor." Cell Metab **9**(1): 23-34.

McCroskery, S., M. Thomas, L. Maxwell, M. Sharma and R. Kambadur (2003). "Myostatin negatively regulates satellite cell activation and self-renewal." J Cell Biol **162**(6): 1135-1147.

McFarlane, C., E. Plummer, M. Thomas, A. Hennebry, M. Ashby, N. Ling, H. Smith, M. Sharma and R. Kambadur (2006). "Myostatin induces cachexia by activating the ubiquitin proteolytic system through an NF-kappaB-independent, FoxO1-dependent mechanism." Journal of cellular physiology **209**(2): 501-514.

McPherron, A. C., T. V. Huynh and S. J. Lee (2009). "Redundancy of myostatin and growth/differentiation factor 11 function." BMC developmental biology **9**: 24.

McPherron, A. C., A. M. Lawler and S. J. Lee (1997). "Regulation of skeletal muscle mass in mice by a new TGF-beta superfamily member." Nature **387**(6628): 83-90.

McPherron, A. C. and S. J. Lee (2002). "Suppression of body fat accumulation in myostatin-deficient mice." The Journal of clinical investigation **109**(5): 595-601.

Mendias, C. L., J. E. Marcin, D. R. Calerdon and J. A. Faulkner (2006). "Contractile properties of EDL and soleus muscles of myostatin-deficient mice." Journal of applied physiology **101**(3): 898-905.

Menissier, F. (1982). Muscle Hypertrophy of Genetic Origin and Its Use to Improve Beef Production. The Hague, Martinus Nijhoff.

Milan, G., E. Dalla Nora, C. Pilon, C. Pagano, M. Granzotto, M. Manco, G. Mingrone and R. Vettor (2004). "Changes in muscle myostatin expression in obese subjects after weight loss." The Journal of clinical endocrinology and metabolism **89**(6): 2724-2727.

Mitchell, M. D., C. C. Osepchook, K. C. Leung, C. D. McMahon and J. J. Bass (2006). "Myostatin is a human placental product that regulates glucose uptake." The Journal of clinical endocrinology and metabolism **91**(4): 1434-1437.

Morine, K. J., L. T. Bish, K. Pendrak, M. M. Sleeper, E. R. Barton and H. L. Sweeney (2010). "Systemic myostatin inhibition via liver-targeted gene transfer in normal and dystrophic mice." PloS one **5**(2): e9176.

Morissette, M. R., S. A. Cook, C. Buranasombati, M. A. Rosenberg and A. Rosenzweig (2009). "Myostatin inhibits IGF-I-induced myotube hypertrophy through Akt." American journal of physiology. Cell physiology **297**(5): C1124-1132.

Mosher, D. S., P. Quignon, C. D. Bustamante, N. B. Sutter, C. S. Mellersh, H. G. Parker and E. A. Ostrander (2007). "A mutation in the myostatin gene increases muscle mass and enhances racing performance in heterozygote dogs." PLoS genetics **3**(5): e79.

Mukherjee, A., Y. Sidis, A. Mahan, M. J. Raher, Y. Xia, E. D. Rosen, K. D. Bloch, M. K. Thomas and A. L. Schneyer (2007). "FSTL3 deletion reveals roles for TGF-beta family ligands in glucose and fat homeostasis in adults." Proceedings of the National Academy of Sciences of the United States of America **104**(4): 1348-1353.

Musaro, A., K. McCullagh, A. Paul, L. Houghton, G. Dobrowolny, M. Molinaro, E. R. Barton, H. L. Sweeney and N. Rosenthal (2001). "Localized Igf-1 transgene expression sustains hypertrophy and regeneration in senescent skeletal muscle." Nature genetics **27**(2): 195-200.

Ojuka, E. O. (2004). "Role of calcium and AMP kinase in the regulation of mitochondrial biogenesis and GLUT4 levels in muscle." Proc Nutr Soc **63**(2): 275-278.

Ojuka, E. O., T. E. Jones, D. H. Han, M. Chen, B. R. Wamhoff, M. Sturek and J. O. Holloszy (2002). "Intermittent increases in cytosolic Ca2+ stimulate mitochondrial biogenesis in muscle cells." Am J Physiol Endocrinol Metab **283**(5): E1040-1045.

Ojuka, E. O., T. E. Jones, L. A. Nolte, M. Chen, B. R. Wamhoff, M. Sturek and J. O. Holloszy (2002). "Regulation of GLUT4 biogenesis in muscle: evidence for involvement of AMPK and Ca(2+)." Am J Physiol Endocrinol Metab **282**(5): E1008-1013.

Palsgaard, J., C. Brons, M. Friedrichsen, H. Dominguez, M. Jensen, H. Storgaard, C. Spohr, C. Torp-Pedersen, R. Borup, P. De Meyts and A. Vaag (2009). "Gene expression in skeletal muscle biopsies from people with type 2 diabetes and relatives: differential regulation of insulin signaling pathways." PloS one **4**(8): e6575.

Park, J. J., J. R. Berggren, M. W. Hulver, J. A. Houmard and E. P. Hoffman (2006). "GRB14, GPD1, and GDF8 as potential network collaborators in weight loss-induced improvements in insulin action in human skeletal muscle." Physiological genomics **27**(2): 114-121.

Patel, K. and H. Amthor (2005). "The function of Myostatin and strategies of Myostatin blockade-new hope for therapies aimed at promoting growth of skeletal muscle." Neuromuscular disorders : NMD **15**(2): 117-126.

Pedersen, B. K. (2009). "Edward F. Adolph distinguished lecture: muscle as an endocrine organ: IL-6 and other myokines." J Appl Physiol **107**(4): 1006-1014.

Pedersen, B. K. and M. A. Febbraio (2008). "Muscle as an endocrine organ: focus on muscle-derived interleukin-6." Physiol Rev **88**(4): 1379-1406.

Perry, R. C. and A. D. Baron (1999). "Impaired glucose tolerance. Why is it not a disease?" Diabetes Care **22**(6): 883-885.

PHAC (2011). Diabetes in Canada: Facts and figures from a public health perspective. Ottawa, ON, Canada, Public Health Agency of Canada

Philip, B., Z. Lu and Y. Gao (2005). "Regulation of GDF-8 signaling by the p38 MAPK." Cell Signal **17**(3): 365-375.

Ploquin, C., B. Chabi, G. Fouret, B. Vernus, C. Feillet-Coudray, C. Coudray, A. Bonnieu and C. Ramonatxo (2012). "Lack of myostatin alters intermyofibrillar mitochondria activity, unbalances redox status, and impairs tolerance to chronic repetitive contractions in muscle." Am J Physiol Endocrinol Metab **302**(8): E1000-1008.

Pold, R., L. S. Jensen, N. Jessen, E. S. Buhl, O. Schmitz, A. Flyvbjerg, N. Fujii, L. J. Goodyear, C. F. Gotfredsen, C. L. Brand and S. Lund (2005). "Long-term AICAR administration and exercise prevents diabetes in ZDF rats." Diabetes **54**(4): 928-934.

Pursel, V. G., A. D. Mitchell, G. Bee, T. H. Elsasser, J. P. McMurtry, R. J. Wall, M. E. Coleman and R. J. Schwartz (2004). "Growth and tissue accretion rates of swine expressing an insulin-like growth factor I transgene." Animal biotechnology **15**(1): 33-45.

Qiao, C., J. Li, J. Jiang, X. Zhu, B. Wang and X. Xiao (2008). "Myostatin propeptide gene delivery by adeno-associated virus serotype 8 vectors enhances muscle growth and ameliorates dystrophic phenotypes in mdx mice." Human gene therapy **19**(3): 241-254.

Rebbapragada, A., H. Benchabane, J. L. Wrana, A. J. Celeste and L. Attisano (2003). "Myostatin signals through a transforming growth factor beta-like signaling pathway to block adipogenesis." Molecular and cellular biology **23**(20): 7230-7242.

Reisz-Porszasz, S., S. Bhasin, J. N. Artaza, R. Shen, I. Sinha-Hikim, A. Hogue, T. J. Fielder and N. F. Gonzalez-Cadavid (2003). "Lower skeletal muscle mass in male transgenic mice with muscle-specific overexpression of myostatin." American journal of physiology. Endocrinology and metabolism **285**(4): E876-888.

Ricaud, S., B. Vernus, M. Duclos, H. Bernardi, O. Ritvos, G. Carnac and A. Bonnieu (2003). "Inhibition of autocrine secretion of myostatin enhances terminal differentiation in human rhabdomyosarcoma cells." Oncogene **22**(51): 8221-8232.

Rios, R., S. Fernandez-Nocelos, I. Carneiro, V. M. Arce and J. Devesa (2004). "Differential response to exogenous and endogenous myostatin in myoblasts suggests that myostatin acts as an autocrine factor in vivo." Endocrinology **145**(6): 2795-2803.

Ruderman, N. B., A. K. Saha, D. Vavvas and L. A. Witters (1999). "Malonyl-CoA, fuel sensing, and insulin resistance." Am J Physiol **276**(1 Pt 1): E1-E18.

Savage, D. B., K. F. Petersen and G. I. Shulman (2007). "Disordered lipid metabolism and the pathogenesis of insulin resistance." Physiological reviews **87**(2): 507-520.

Savage, K. J. and A. C. McPherron (2010). "Endurance exercise training in myostatin null mice." Muscle Nerve **42**(3): 355-362.

Schuelke, M., K. R. Wagner, L. E. Stolz, C. Hubner, T. Riebel, W. Komen, T. Braun, J. F. Tobin and S. J. Lee (2004). "Myostatin mutation associated with gross muscle hypertrophy in a child." The New England journal of medicine **350**(26): 2682-2688.

Shaw, J. E., P. Z. Zimmet, M. de Courten, G. K. Dowse, P. Chitson, H. Gareeboo, F. Hemraj, D. Fareed, J. Tuomilehto and K. G. Alberti (1999). "Impaired fasting glucose or impaired glucose tolerance. What best predicts future diabetes in Mauritius?" Diabetes Care **22**(3): 399-402.

Shulman, G. I., D. L. Rothman, T. Jue, P. Stein, R. A. DeFronzo and R. G. Shulman (1990). "Quantitation of muscle glycogen synthesis in normal subjects and subjects with non-insulin-dependent diabetes by 13C nuclear magnetic resonance spectroscopy." N Engl J Med **322**(4): 223-228.

Souza, T. A., X. Chen, Y. Guo, P. Sava, J. Zhang, J. J. Hill, P. J. Yaworsky and Y. Qiu (2008). "Proteomic identification and functional validation of activins and bone morphogenetic protein 11 as candidate novel muscle mass regulators." Molecular endocrinology **22**(12): 2689-2702.

StatsCan (2005). Population Projections for Canada, Provinces and Territories, 2005-2031. Ottawa, ON, Canada, StatsCan.

Steelman, C. A., J. C. Recknor, D. Nettleton and J. M. Reecy (2006). "Transcriptional profiling of myostatin-knockout mice implicates Wnt signaling in postnatal skeletal muscle growth and hypertrophy." FASEB J **20**(3): 580-582.

Steinberg, G. R., S. L. Macaulay, M. A. Febbraio and B. E. Kemp (2006). "AMP-activated protein kinase--the fat controller of the energy railroad." Canadian journal of physiology and pharmacology **84**(7): 655-665.

Stolz, L. E., D. Li, A. Qadri, M. Jalenak, L. D. Klaman and J. F. Tobin (2008). "Administration of myostatin does not alter fat mass in adult mice." Diabetes, obesity & metabolism **10**(2): 135-142.

Sutrave, P., A. M. Kelly and S. H. Hughes (1990). "ski can cause selective growth of skeletal muscle in transgenic mice." Genes & development **4**(9): 1462-1472.

Tang, L., Z. Yan, Y. Wan, W. Han and Y. Zhang (2007). "Myostatin DNA vaccine increases skeletal muscle mass and endurance in mice." Muscle & nerve **36**(3): 342-348.

Taubes, G. (2009). "Insulin resistance. Prosperity's plague." Science **325**(5938): 256-260.

Thies, R. S., T. Chen, M. V. Davies, K. N. Tomkinson, A. A. Pearson, Q. A. Shakey and N. M. Wolfman (2001). "GDF-8 propeptide binds to GDF-8 and antagonizes biological activity by inhibiting GDF-8 receptor binding." Growth Factors **18**(4): 251-259.

Thomas, M., B. Langley, C. Berry, M. Sharma, S. Kirk, J. Bass and R. Kambadur (2000). "Myostatin, a negative regulator of muscle growth, functions by inhibiting myoblast proliferation." The Journal of biological chemistry **275**(51): 40235-40243.

Thomson, D. M., B. B. Porter, J. H. Tall, H. J. Kim, J. R. Barrow and W. W. Winder (2007). "Skeletal muscle and heart LKB1 deficiency causes decreased voluntary running and reduced muscle mitochondrial marker enzyme expression in mice." Am J Physiol Endocrinol Metab **292**(1): E196-202.

Tominaga, M., H. Eguchi, H. Manaka, K. Igarashi, T. Kato and A. Sekikawa (1999). "Impaired glucose tolerance is a risk factor for cardiovascular disease, but not impaired fasting glucose. The Funagata Diabetes Study." Diabetes Care **22**(6): 920-924.

Trendelenburg, A. U., A. Meyer, D. Rohner, J. Boyle, S. Hatakeyama and D. J. Glass (2009). "Myostatin reduces Akt/TORC1/p70S6K signaling, inhibiting myoblast differentiation and myotube size." American journal of physiology. Cell physiology **296**(6): C1258-1270.

Tsuchida, K., M. Nakatani, T. Matsuzaki, N. Yamakawa, Z. Liu, Y. Bao, K. Y. Arai, T. Murakami, Y. Takehara, A. Kurisaki and H. Sugino (2004). "Novel factors in regulation of activin signaling." Molecular and cellular endocrinology **225**(1-2): 1-8.

Tu, P., S. Bhasin, P. W. Hruz, K. L. Herbst, L. W. Castellani, N. Hua, J. A. Hamilton and W. Guo (2009). "Genetic disruption of myostatin reduces the development of proatherogenic dyslipidemia and atherogenic lesions in Ldlr null mice." Diabetes **58**(8): 1739-1748.

Walsh, F. S. and A. J. Celeste (2005). "Myostatin: a modulator of skeletal-muscle stem cells." Biochemical Society transactions **33**(Pt 6): 1513-1517.

Warram, J. H., B. C. Martin, A. S. Krolewski, J. S. Soeldner and C. R. Kahn (1990). "Slow glucose removal rate and hyperinsulinemia precede the development of type II diabetes in the offspring of diabetic parents." Annals of internal medicine **113**(12): 909-915.

Welle, S., K. Bhatt, C. A. Pinkert, R. Tawil and C. A. Thornton (2007). "Muscle growth after postdevelopmental myostatin gene knockout." American journal of physiology. Endocrinology and metabolism **292**(4): E985-991.

Welle, S., A. Cardillo, M. Zanche and R. Tawil (2009). "Skeletal muscle gene expression after myostatin knockout in mature mice." Physiological genomics **38**(3): 342-350.

Whittemore, L. A., K. Song, X. Li, J. Aghajanian, M. Davies, S. Girgenrath, J. J. Hill, M. Jalenak, P. Kelley, A. Knight, R. Maylor, D. O'Hara, A. Pearson, A. Quazi, S. Ryerson, X. Y. Tan, K. N. Tomkinson, G. M. Veldman, A. Widom, J. F. Wright, S. Wudyka, L. Zhao and N. M. Wolfman (2003). "Inhibition of myostatin in adult mice increases skeletal muscle mass and strength." Biochemical and biophysical research communications **300**(4): 965-971.

WHO (September 2012). Fact sheet N°312. Media Centre, WHO.

Wilkes, J. J., D. J. Lloyd and N. Gekakis (2009). "Loss-of-function mutation in myostatin reduces tumor necrosis factor alpha production and protects liver against obesity-induced insulin resistance." Diabetes **58**(5): 1133-1143.

Williams, M. S. (2004). "Myostatin mutation associated with gross muscle hypertrophy in a child." The New England journal of medicine **351**(10): 1030-1031; author reply 1030-1031.

Winder, W. W. (2000). "AMP-activated protein kinase: possible target for treatment of type 2 diabetes." Diabetes Technol Ther **2**(3): 441-448.

Winder, W. W. (2001). "Energy-sensing and signaling by AMP-activated protein kinase in skeletal muscle." J Appl Physiol **91**(3): 1017-1028.

Winder, W. W., B. F. Holmes, D. S. Rubink, E. B. Jensen, M. Chen and J. O. Holloszy (2000). "Activation of AMP-activated protein kinase increases mitochondrial enzymes in skeletal muscle." J Appl Physiol **88**(6): 2219-2226.

Wolfman, N. M., A. C. McPherron, W. N. Pappano, M. V. Davies, K. Song, K. N. Tomkinson, J. F. Wright, L. Zhao, S. M. Sebald, D. S. Greenspan and S. J. Lee (2003). "Activation of latent myostatin by the BMP-1/tolloid family of metalloproteinases." Proceedings of the National Academy of Sciences of the United States of America **100**(26): 15842-15846.

Yamauchi, T., J. Kamon, Y. Minokoshi, Y. Ito, H. Waki, S. Uchida, S. Yamashita, M. Noda, S. Kita, K. Ueki, K. Eto, Y. Akanuma, P. Froguel, F. Foufelle, P. Ferre, D. Carling, S. Kimura, R. Nagai, B. B. Kahn and T. Kadowaki (2002). "Adiponectin stimulates glucose utilization and fatty-acid oxidation by activating AMP-activated protein kinase." Nat Med **8**(11): 1288-1295.

Yang, W., Y. Zhang, Y. Li, Z. Wu and D. Zhu (2007). "Myostatin induces cyclin D1 degradation to cause cell cycle arrest through a phosphatidylinositol 3-kinase/Akt/GSK-3 beta pathway and is antagonized by insulin-like growth factor 1." The Journal of biological chemistry **282**(6): 3799-3808.

Zhang, C., C. McFarlane, S. Lokireddy, S. Bonala, X. Ge, S. Masuda, P. D. Gluckman, M. Sharma and R. Kambadur (2011). "Myostatin-deficient mice exhibit reduced insulin resistance through activating the AMP-activated protein kinase signalling pathway." Diabetologia **54**(6): 1491-1501.

Zhang, L., M. Frederich, H. He and J. A. Balschi (2006). "Relationship between 5-aminoimidazole-4-carboxamide-ribotide and AMP-activated protein kinase activity in the perfused mouse heart." Am J Physiol Heart Circ Physiol **290**(3): H1235-1243.

Zhu, X., M. Hadhazy, M. Wehling, J. G. Tidball and E. M. McNally (2000). "Dominant negative myostatin produces hypertrophy without hyperplasia in muscle." FEBS letters **474**(1): 71-75.

Zhu, X., S. Topouzis, L. F. Liang and R. L. Stotish (2004). "Myostatin signaling through Smad2, Smad3 and Smad4 is regulated by the inhibitory Smad7 by a negative feedback mechanism." Cytokine **26**(6): 262-272.

Zimmers, T. A., M. V. Davies, L. G. Koniaris, P. Haynes, A. F. Esquela, K. N. Tomkinson, A. C. McPherron, N. M. Wolfman and S. J. Lee (2002). "Induction of cachexia in mice by systemically administered myostatin." Science **296**(5572): 1486-1488.

Zong, H., J. M. Ren, L. H. Young, M. Pypaert, J. Mu, M. J. Birnbaum and G. I. Shulman (2002). "AMP kinase is required for mitochondrial biogenesis in skeletal muscle in response to chronic energy deprivation." Proc Natl Acad Sci U S A **99**(25): 15983-15987.